New Phytologist

International Journal of Plant Science

TANSLEY INSIGHTS

Several geranylgeranyl diphosphate synthase isoforms supply metabolic substrates for carotenoid biosynthesis in tomato

M. Victoria Barja[1]* (iD), Miguel Ezquerro[1],* (iD), Stefano Beretta[1], Gianfranco Diretto[2] (iD), Igor Florez-Sarasa[1] (iD), Elisenda Feixes[1] (iD), Alessia Fiore[2], Rumyana Karlova[3] (iD), Alisdair R. Fernie[4] (iD), Jules Beekwilder[5] (iD) and Manuel Rodríguez-Concepción[1,6] (iD)

[1]Centre for Research in Agricultural Genomics (CRAG) CSIC-IRTA-UAB-UB, Campus UAB Bellaterra, Barcelona 08193, Spain; [2]Italian National Agency for New Technologies, Energy, and Sustainable Development, Casaccia Research Centre, Rome 00123, Italy; [3]Laboratory of Plant Physiology, Wageningen University and Research, Wageningen 6700AA, the Netherlands; [4]Max-Planck-Institut für Molekulare Pflanzenphysiologie, Potsdam-Golm 14476, Germany; [5]BU Bioscience, Wageningen University and Research, Wageningen 6700AA, the Netherlands; [6]Institute for Plant Molecular and Cell Biology (IBMCP), CSIC-Universitat Politècnica de València, València 46022, Spain

Summary

• Geranylgeranyl diphosphate (GGPP) produced by GGPP synthase (GGPPS) serves as a precursor for many plastidial isoprenoids, including carotenoids. Phytoene synthase (PSY) converts GGPP into phytoene, the first committed intermediate of the carotenoid pathway.
• Here we used biochemical, molecular, and genetic tools to characterise the plastidial members of the GGPPS family in tomato (*Solanum lycopersicum*) and their interaction with PSY isoforms.
• The three tomato GGPPS isoforms found to localise in plastids (SlG1, 2 and 3) exhibit similar kinetic parameters. Gene expression analyses showed a preferential association of individual GGPPS and PSY isoforms when carotenoid biosynthesis was induced during root mycorrhization, seedling de-etiolation and fruit ripening. SlG2, but not SlG3, physically interacts with PSY proteins. By contrast, CRISPR-Cas9 mutants defective in SlG3 showed a stronger impact on carotenoid levels and derived metabolic, physiological and developmental phenotypes compared with those impaired in SlG2. Double mutants defective in both genes could not be rescued.
• Our work demonstrates that the bulk of GGPP production in tomato chloroplasts and chromoplasts relies on two cooperating GGPPS paralogues, unlike other plant species such as *Arabidopsis thaliana*, rice or pepper, which produce their essential plastidial isoprenoids using a single GGPPS isoform.

Introduction

Isoprenoids are essential biological molecules in all living organisms. In particular, plants are the main source of the enormous structural and functional variety that characterises this family of compounds (Pulido *et al.*, 2012; Tholl, 2015). The building blocks for the biosynthesis of all isoprenoids are isopentenyl diphosphate (IPP) and its double-bond isomer dimethylallyl diphosphate (DMAPP). These five-carbon (C5) universal isoprenoid units are produced in plants through the mevalonic acid (MVA) pathway in the cytosol and the methylerythritol 4-phosphate (MEP) pathway in plastids (Vranová *et al.*, 2013; Rodríguez-Concepción & Boronat, 2015). Short-chain prenyltransferases subsequently condense one or more molecules of IPP to one molecule of DMAPP giving rise to C10, C15, C20 and C25 prenyl diphosphates, known as geranyl diphosphate (GPP),

farnesyl diphosphate (FPP), geranylgeranyl diphosphate (GGPP), and geranylfarnesyl diphosphate (GFPP), respectively. These molecules are the immediate precursors for downstream pathways leading to the production of the main groups of isoprenoids.

Carotenoids are one of the most studied groups of plant isoprenoids. These C40 tetraterpenes are greatly demanded by cosmetic and agro-food industries as natural red to yellow pigments and provide benefits for human health, for example as precursors of vitamin A and other biologically active molecules (Sandmann, 2015; Rodríguez-Concepción *et al.*, 2018). In plants, carotenoids have different functions. In photosynthetic tissues, they are required for the assembly of the photosynthetic apparatus, contribute to light harvesting and are essential for photoprotection by dissipating excess light energy as heat and by scavenging reactive oxygen species. They are also fundamental in growth regulation as they are the precursors of retrograde signals and phytohormones such as abscisic acid (ABA) and strigolactones. As a secondary role, carotenoids provide distinctive colours to flowers and fruits to

*These authors contributed equally to this work.

attract pollinators and seed dispersal animals (Nisar *et al.*, 2015; Yuan *et al.*, 2015). In plants, carotenoids are produced and stored in plastids, including chloroplasts and chromoplasts (Ruiz-Sola & Rodríguez-Concepción, 2012; Sun *et al.*, 2018). MEP-derived IPP and DMAPP are converted into GGPP by plastidial GGPP synthase (GGPPS) isoforms and then GGPP is transformed into phytoene by phytoene synthase (PSY) enzymes. The production of phytoene, the first committed intermediate of the carotenoid pathway, is considered to be a major rate-determining step regulating the metabolic flux through this pathway (Fraser *et al.*, 2002). In tomato (*Solanum lycopersicum*), three PSY-encoding genes control carotenoid biosynthesis in different tissues. *PSY1* expression is boosted during ripening to produce carotenoids involved in the pigmentation of the fruit (Bartley *et al.*, 1992; Fray & Grierson, 1993; Giorio *et al.*, 2008; Kachanovsky *et al.*, 2012). *PSY2* is expressed in all tissues, including fruits, but transcript levels are much higher than those of *PSY1* in photosynthetic tissues, where carotenoids are required for photosynthesis and photoprotection (Bartley & Scolnik, 1993; Giorio *et al.*, 2008). Lastly, *PSY3* is mainly expressed in roots and it is induced during mycorrhization (Walter *et al.*, 2015; Stauder *et al.*, 2018), when carotenoid biosynthesis is upregulated to produce strigolactones and apocarotenoid molecules essential for the establishment of the symbiosis (Fester *et al.*, 2002, 2005; Baslam *et al.*, 2013; Ruiz-Lozano *et al.*, 2016; Stauder *et al.*, 2018). Whether the corresponding PSY isoforms use GGPP supplied by different GGPPS isoforms remains unknown.

Several GGPPS paralogues have been retained in plants during evolution (Beck *et al.*, 2013; Zhang *et al.*, 2015; Ruiz-Sola *et al.*, 2016a,b; Zhou *et al.*, 2017; Wang *et al.*, 2018). However, a single GGPPS isoform appears to produce the GGPP substrate needed for the production of carotenoids and other plastidial isoprenoids in *Arabidopsis thaliana,* rice (*Oryza sativa*) and pepper (*Capsicum annuum*), the three plant species whose GGPPS families have been best characterised to date (Ruiz-Sola *et al.*, 2016a, b; Zhou *et al.*, 2017; Wang *et al.*, 2018). While tomato has become a model plant systems to study the biosynthesis of carotenoids and its regulation, we still have an incomplete picture of the GGPPS family in this plant. Recent work has determined that five genes encoding GGPPS homologues exist in the tomato genome, three of which were confirmed to produce GGPP *in vitro* and localise in plastids (Zhou & Pichersky, 2020). Which of these plastidial GGPPS isoforms are required for the production of carotenoids in photosynthetic tissues (e.g. for photoprotection), fruits (e.g. for pigmentation) or roots (e.g. for mycorrhization) remains unknown. Here we characterised the *in vivo* role of these plastidial GGPPS enzymes and provide clues to understand how the supply of plastidial GGPP for the synthesis of carotenoids with different biological functions in particular tomato tissues is regulated in this important crop plant.

Materials and Methods

Plant material

Tomato (*Solanum lycopersicum* var. MicroTom) plants were used for most experiments. Seed germination, plant growth and sample collection were carried out as described (Supporting Information Methods S1). *Agrobacterium tumefaciens* GV3101 strain was used to stably transform tomato MicroTom cotyledons with plasmids harbouring two sgRNAs to disrupt *SlG2* and *SlG3* genomic sequences as described previously (Fernandez *et al.*, 2009). The sgRNAs were designed for each gene to create short deletions using the CRISPR P 2.0 online tool (http://crispr.hzau.edu.cn/CRISPR2/; Liu *et al.*, 2017). Cloning of the sgRNA sequences was performed as described previously (Schiml *et al.*, 2016) using a pDE-Cas9 plasmid providing kanamycin resistance (Methods S2). Primers and cloning steps are detailed in Tables S1 and S2, respectively. *In vitro* regenerated T1 lines were identified based on kanamycin resistance (100 µg ml^{-1}), PCR genotyping and restriction analyses. Homozygous T2 lines lacking Cas9 were obtained after segregation. Stable T3 offspring was used for further experiments. Methods S2 and Tables S1 and S2 describe the generation of the rest of the constructs. *Nicotiana benthamiana* plants were grown and used for transient expression assays (agroinfiltration) as previously described (Llorente *et al.*, 2020).

Gene co-expression network (GCN) analyses

GCN analyses were performed as previously described (Ahrazem *et al.*, 2018). Pairwise Pearson correlations between each GGPPS gene and each selected isoprenoid biosynthetic input gene were computed for leaf and fruit tissues throughout their development and Fisher's Z-transformation was used to test their statistical significance.

RNA analyses

RNA isolation, cDNA synthesis, and RT-qPCR analyses were carried out as described (Methods S3). Normalised transcript abundances were calculated as described previously (Simon, 2003) using tomato *ACT4* (*Solyc04g011500*) or *EXP* (*Solyc07g025390*) as endogenous reference genes. Three biological replicates of cDNA samples from roots of nonmycorrhized and mycorrhized tomato plants (Ruiz-Lozano *et al.*, 2016) were kindly provided by Juan Antonio López-Ráez.

Protein analyses

In vitro GGPPS activity determination was performed as described (Methods S4). Purified enzymes were used to calculate kinetic parameters as described previously (Barja & Rodríguez-Concepción, 2020). Protein concentration was determined according to the Bradford method (Bradford, 1976). GGPPS activity assays in *E. coli* were carried out as described previously (Beck *et al.*, 2013). Subcellular localisation assays were performed using *A. tumefaciens*-mediated transient expression in *N. benthamiana* leaves (Sparkes *et al.*, 2006). Leaves were co-infiltrated with strains carrying appropriate constructs (Methods S2) and a HC-Pro silencing suppressor (Goytia *et al.*, 2006) as described (Methods S5). Subcellular localisation of GFP fusion proteins was determined 3 d post infiltration with an Olympus

FV 1000 confocal laser-scanning microscope (Methods S5). Co-immunoprecipitation (Co-IP) assays were performed in *N. benthamiana leaves* as described previously (Muñoz & Castellano, 2018; Methods S6). Immunoblot analyses were performed as described previously (Pulido *et al.*, 2013).

Metabolite analysis

Detection of prenyl diphosphates was carried out as described previously (Ruiz-Sola *et al.*, 2016a). Carotenoids, chlorophylls and tocopherols were extracted as described (Methods S7). Separation and detection were next performed using an Agilent 1200 series HPLC system (Agilent Technologies) as previously reported (Fraser *et al.*, 2000). ABA levels were determined as described previously (Diretto *et al.*, 2020). Primary metabolites were extracted, annotated and quantified as described previously (Llorente *et al.*, 2020).

Results

SlG1, SlG2 and SlG3 are GGPP-producing plastidial enzymes with similar kinetic properties

Several genes encoding proteins with homology to GGPPS enzymes are found in the tomato genome (Ament *et al.*, 2006; Fraser *et al.*, 2007; Stauder *et al.*, 2018; Zhou & Pichersky, 2020). From these, three have been found to localise in plastids and produce GGPP *in vitro*, namely *GGPPS1* (*Solyc11g011240*), *GGPPS2* (*Solyc04g079960*) and *GGPPS3* (*Solyc02g085700*), here referred to as *SlG1*, *SlG2* and *SlG3* (Table S3). We confirmed the plastidial targeting of these three isoforms by expressing constructs encoding GFP fusions of the full-length SlG1-3 proteins in agroinfiltrated tobacco (*Nicotiana benthamiana*) leaves. In all three cases, fluorescence corresponding to the GFP fusion proteins co-localised with chlorophyll autofluorescence (Fig. S1), and supported the conclusion that they were all efficiently targeted to chloroplasts. We also experimentally confirmed the ability of purified SlG1-3 proteins to produce GGPP *in vitro*. The three tomato isoforms were expressed in *Escherichia coli* cells without their predicted plastid-targeting sequences (Fig. S2) and whole-cell protein extracts were directly used for activity assays in the presence of IPP and DMAPP followed by the analysis of the reaction products by LC-MS (Fig. S3). As positive and negative controls, we used the Arabidopsis AtG11 (active) and AtG11s (inactive) proteins (Ruiz-Sola *et al.*, 2016a). This experiment confirmed that SlG1, SlG2, SlG3 and AtG11 (but no AtG11s) produced only GGPP (Fig. S3a), in agreement with recently reported data (Zhou & Pichersky, 2020). To gain new knowledge on the biochemical properties of these enzymes, we used purified proteins to calculate their kinetic parameters. Enzymatic assays performed as described previously (Barja & Rodríguez-Concepción, 2020) showed that all tested GGPPS proteins exhibited a similar optimal pH around 7.5 (Fig. S3b), as expected for stromal enzymes (Höhner *et al.*, 2016). The parameters Km (an estimator of the apparent affinity for the IPP and DMAPP substrates) and Vmax exhibited very similar values among the three tomato enzymes (Table 1). They were also similar to those obtained for AtG11 here and elsewhere (Wang & Dixon, 2009; Camagna *et al.*, 2019). We therefore concluded that tomato SlG1, SlG2 and SlG3 and Arabidopsis AtG11 are plastidial GGPPS enzymes with very similar kinetic properties.

Gene expression profiles suggest a major role of SlG2 and SlG3 in chloroplasts and chromoplasts

Analysis of public gene expression databases showed that the genes encoding SlG1-3 enzymes were expressed in roots, leaves and flowers (Fig. S4). Of these, the most highly expressed gene was *SlG3* followed by *SlG2*, while *SlG1* transcripts were present at very low levels. *SlG2* and *SlG3*, but not *SlG1,* were also expressed at high levels in fruit pericarp and seed tissues (Fig. S4). As an initial approach to gain an insight into the possible functions of these individual isoforms, we performed a GCN analysis. This is a powerful tool to infer biological functions that we previously used to identify AtG11 as the main GGPPS isoform for plastidial isoprenoid production in Arabidopsis (Ruiz-Sola *et al.*, 2016b). By using publicly available databases for plant comparative genomics (*PLAZA 4.0*, *Phytozome*), we searched for tomato homologues of the plastidial pathways that supply GGPPS substrates (MEP pathway) and consume GGPP to produce carotenoids, chlorophylls, tocopherols, phylloquinone, plastoquinone, gibberellins, strigolactones and ABA (Table S4). We retrieved their expression data from TomExpress database (Zouine *et al.*, 2017) experiments carried out using either leaf or fruit samples at different developmental stages (Table S5). Then, we calculated their correlation with *SlG1, SlG2* and *SlG3* expression using pairwise Pearson correlations. The results of the GCN analyses are shown in Fig. 1 and Fig. S5, and correlations are listed in Table S6. It was not possible to obtain correlation data for tomato roots as only two experiments using root samples are deposited in the TomExpress database. In leaves and fruits, *SlG1* was poorly co-expressed with the query genes. By contrast, and similar to that observed with *AtG11* (Ruiz-Sola *et al.*, 2016b)*, SlG2* and, to a lower extent, *SlG3* were highly connected to plastidial isoprenoid biosynthetic genes in leaf tissues. Connectivity was lower in fruit and, in this case, it was a bit higher for *SlG3* (Fig. 1). These results suggest that SlG2 and SlG3 might be the main GGPP-producing isoforms in leaf chloroplasts and fruit chromoplasts.

In tomato, carotenoids contribute to mycorrhizal associations, photoprotection and fruit pigmentation and, therefore, the levels of these GGPP-derived metabolites increase during root mycorrhization, seedling de-etiolation and fruit ripening. In agreement with the rate-determining role of PSY for carotenoid synthesis (Fraser *et al.*, 2002), the expression levels of PSY-encoding genes also increase during such carotenoid-demanding developmental processes. By using real-time quantitative PCR (qPCR) analysis, we experimentally confirmed the upregulation of *PSY1* during fruit ripening and *PSY3* in mycorrhized roots (Fig. 2). Furthermore, we found that the *PSY2* gene was more strongly upregulated than *PSY1* during tomato seedling de-etiolation (Fig. 2). Using the same samples, we observed that only *SlG1* was

Table 1 Kinetic parameters of tomato plastidial GGPPS enzymes.

	DMAPP (+100 μM IPP)		IPP (+100 μM DMAPP)	
	Km (μM)	V_{max} (nmol min^{-1} mg^{-1})	Km (μM)	V_{max} (nmol min^{-1} mg^{-1})
SlG1	31.82 ± 2.92	47.47 ± 1.40	74.18 ± 7.55	59.87 ± 2.73
SlG2	49.55 ± 5.31	38.87 ± 1.53	79.75 ± 8.33	36.73 ± 1.73
SlG3	45.75 ± 6.81	26.13 ± 1.40	45.92 ± 4.86	29.13 ± 1.13
AtG11	32.86 ± 4.86	21.53 ± 1.07	38.49 ± 4.94	24.13 ± 1.07

Values correspond to the mean ± SD of three independent experimental replicates ($n = 3$).

upregulated during root mycorrhization, showing an expression pattern similar to that observed for *PSY3* (Fig. 2). During fruit ripening, *SlG2* and, to a lower extent, *SlG3* were upregulated, but not as much as *PSY1* (Fig. 2). *SlG2* was also the most strongly upregulated GGPPS-encoding gene during seedling de-etiolation, paralleling *PSY2* induction. Interestingly, *SlG3* and *PSY1* were also induced with a similar profile during this process, even though induction levels were much lower than those observed for *SlG2* and *PSY2* (Fig. 2). Together, these data suggested that SlG1 might provide GGPP for PSY3 to produce carotenoids in roots, particularly when needed during mycorrhization, whereas both SlG2 and SlG3 would be required in leaves and fruits to support carotenoid production for photosynthesis (mostly by PSY2) and fruit pigmentation (by PSY1).

SlG2, but not SlG3, can interact with PSY1 and PSY2

A coordinated role for SlG1 and PSY3 in mycorrhization has already been proposed (Stauder *et al.*, 2018), but the possible connection between the other plastidial GGPPS and PSY isoforms remains unclear. GGPPS proteins can physically interact with PSY and other enzymes catalysing both upstream and downstream biosynthetic steps in the plastids of different plant species (Maudinas *et al.*, 1977; Dogbo & Camara, 1987; Camara, 1993; Fraser *et al.*, 2000; Ruiz-Sola *et al.*, 2016b; Zhou *et al.*, 2017; Wang *et al.*, 2018; Camagna *et al.*, 2019). This mechanism may facilitate channelling of precursors towards specific groups of plastidial isoprenoids. Protein complexes containing both GGPPS and PSY enzymes were isolated from tomato chloroplasts and fruit chromoplasts (Maudinas *et al.*, 1977; Fraser *et al.*, 2000), but the specific isoforms forming these protein complexes were never identified. Given the co-regulation of *SlG2* and *SlG3* with *PSY1* and *PSY2* genes in chloroplasts (i.e. photosynthetic tissues) and chromoplasts (i.e. fruits), we decided to test possible interactions of these isoforms in co-immunoprecipitation assays (Fig. 3). Constructs harbouring C-terminal Myc-tagged GGPPS and HA-tagged PSY sequences were combined and transiently co-expressed in *N. benthamiana* leaves. As a negative control, we used a Myc-tagged version of Arabidopsis phosphoribulokinase (PRK-Myc), a stromal enzyme of the Calvin cycle. Both PSY1-HA and PSY2-HA could be co-immunoprecipitated with SlG2-Myc, suggesting that they are present in the same complexes *in vivo* (Fig. 3). By contrast, none of these PSY isoforms could be

detected in the samples co-immunoprecipitated with either SlG3-Myc or PRK-Myc. The same Myc-tagged SlG2 and SlG3 proteins used in these experiments were able to co-immunoprecipitate their HA-tagged counterparts (Fig. 3). This result, consistent with the ability of GGPPS proteins to form homodimers and also heterodimers, confirms that the observed lack of interaction of SlG3 with PSY enzymes was not due to SlG3-Myc having lost its capacity to interact with other proteins.

Loss of function mutants defective in SlG3, but not those impaired in SlG2, show lower levels of photosynthetic pigments and activity

To further explore the biological roles of SlG2 and SlG3, we generated CRISPR-Cas9 mutants defective in these enzymes (Fig. 4). We designed two single guide RNAs (sgRNA) for each gene with the aim of creating deletions encompassing unique restriction sites for rapid screening (Fig. 4a). Two independent deletion alleles that created premature translation stop codons were selected for each gene and named *slg2-1*, *slg2-2*, *slg3-1* and *slg3-2* (Figs 4a, S6–S8). To confirm that the truncated proteins lacked GGPPS activity, we tested them in *E. coli* strains that synthesised the red carotenoid lycopene only when a source of GGPP was supplied (Ruiz-Sola *et al.*, 2016a). Transformation with constructs harbouring the mutant enzymes did not produce more lycopene than empty plasmid controls, indicating that they lacked GGPPS activity. (Fig. 4b). Once confirmed that the selected mutant alleles produced nonfunctional proteins, homozygous lines without Cas9 were obtained and used for further experiments.

The most obvious phenotype among the selected lines was the pale colour of *slg3* mutants compared with *slg2* alleles or azygous (wild-type (WT)) plants (Fig. 5). This phenotype was clear in emerging and young leaves, but it weakened as leaves grew and became mature (Fig. 5a). The pale colour correlated with significantly reduced levels of carotenoids and chlorophylls in young leaves of *sgl3-1* and *sgl3-2* lines compared with those of WT plants (Fig. 5b; Table S7). The differences were less clear for tocopherols, another group of GGPP-derived plastidial isoprenoids (Fig. 5b). Similar levels of carotenoids, chlorophylls and tocopherols were detected in mature leaves of WT, *slg2* and *slg3* plants (Fig. 5b; Table S7). To test whether the reduced accumulation of photosynthesis-related isoprenoids in *slg3* lines had an impact on photosynthesis, we quantified the effective quantum
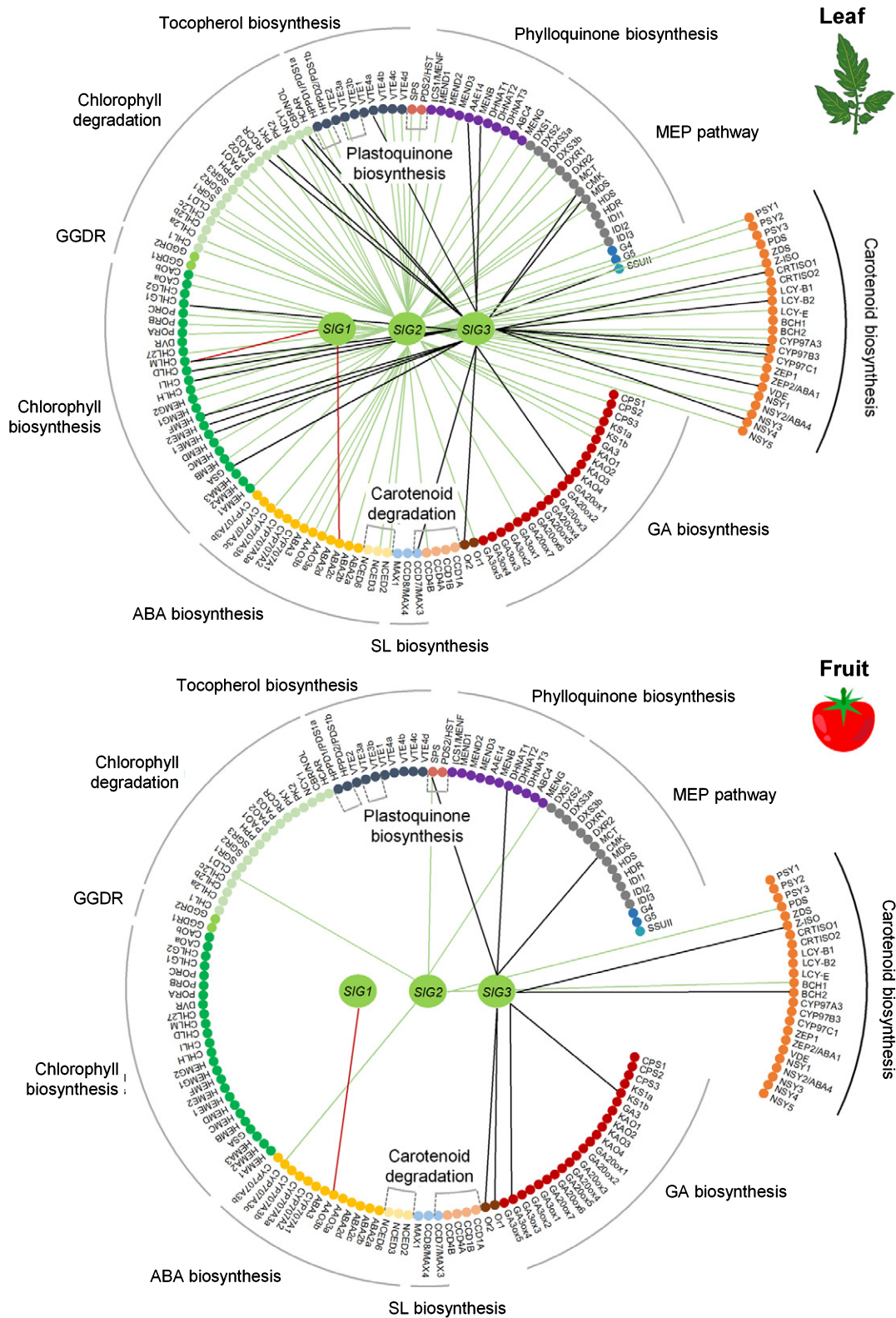
Fig. 1 Gene co-expression analysis of tomato genes encoding plastidial GGPPS isoforms in leaf and fruit tissues. Positive co-expression relationships ($P \geq 0.55$) are depicted in tissue-specific networks as edges. *SIG1*, *SIG2* and *SIG3* are depicted as central green nodes. Surrounding smaller nodes represent genes from the indicated isoprenoid pathways. Red, green and black edges indicate positive co-expression with *SIG1*, *SIG2* and *SIG3* genes, respectively. See Supporting Information Table S4 for gene accessions, Table S5 for leaf and fruit datasets used, and Table S6 for *P*-values.

Fig. 2 Expression profiles of genes encoding tomato PSY and GGPPS paralogues during processes involving increased carotenoid production. First column corresponds to nonmycorrhized (−) and mycorrhize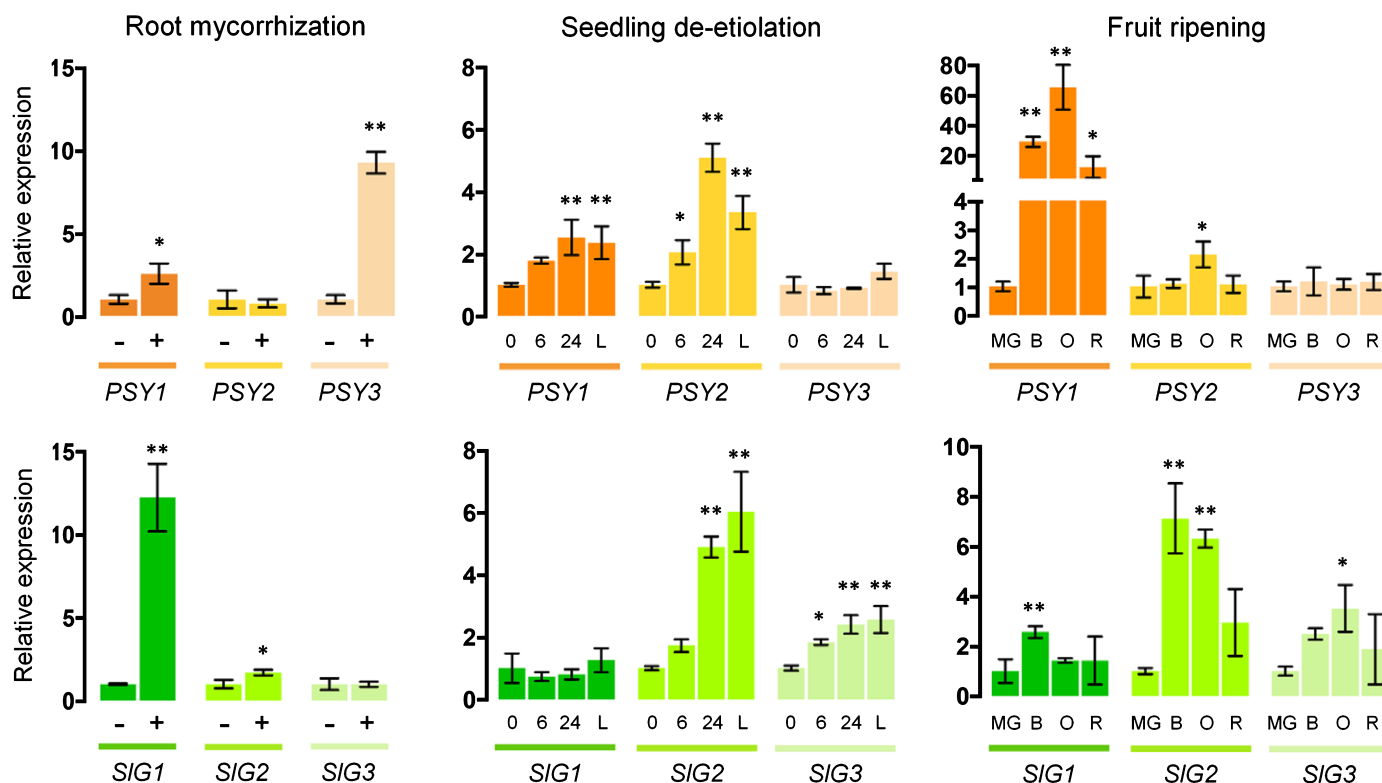d roots (+) at 6 wk postinoculation. Transcript levels were normalised using the tomato *EXP* gene and are shown relative to untreated root samples. Central column samples correspond to 7-d-old dark-grown seedlings at 0, 6 or 24 h after exposure to light and to seedlings continuously grown in the light (L). Transcript levels were normalised to the *EXP* gene and are represented relative to etiolated (0 h) samples. The third column depicts different fruit ripening stages: MG, mature green; B, breaker; O, orange; and R, red ripe. Levels were normalised using *ACT4* and are shown relative to MG samples. Expression values represent the mean ± SD of three independent biological replicates ($n = 3$). Asterisks indicate statistically significant differences relative to untreated (−), etiolated (0 h) or MG samples (*t*-test or one-way ANOVA with Dunnett's multiple comparisons test: *, $P < 0.05$; **, $P < 0.01$).

yield of photosystem II (ϕPSII) in both young and mature leaves (Fig. 5c). A 30% reduction in ϕPSII was observed in young leaves from *slg3* plants compared with those of WT or *slg2* lines, consistent with the *slg3*-specific reduction of GGPP-derived metabolites. Despite similar levels of photosynthetic pigments accumulated in the mature leaves of all genotypes tested, ϕPSII was slightly reduced in some mutants relative to WT lines (Fig. 5c).

We further explored the possible effects that the loss of SlG2 or SlG3 function might have on other metabolic pathways using the same samples of young leaves used for isoprenoid and ϕPSII determination (Fig. 6). GC-MS metabolite profiling showed strongly decreased levels of sucrose, glucose and fructose in SlG3-defective leaves, probably due to photosynthetic impairment. Mutant *slg3* leaves also displayed increased levels of amino acids derived from glycerate (Ser and Gly), shikimate (Phe, Trp and Tyr), pyruvate (Val, Ile and Ala), 2-oxoglutarate (Glu, Orn, His and GABA) and malate (Asp, Asn, Lys, Thr, Met, homoserine and beta-alanine). In line with some of these amino acid changes, SlG3-defective leaves displayed altered accumulation of tricarboxylic acid cycle-related intermediates (citrate and 2-oxoglutarate). Only a few common changes were detected in both *slg2* and *slg3* leaves. They included a decrease in putrescine and

ascorbate levels (more pronounced in *slg3* leaves), as well as an altered accumulation of metabolites produced by the plastidial shikimate pathway, including the above-mentioned aromatic amino acids and phenylpropanoid derivatives such as caffeate and 3-caffeoyl-quinate (Fig. 6). The levels of the carotenoid-derived hormone ABA were similar in WT and mutant samples (Fig. 6; Table 2).

Ripening-associated fruit pigmentation is altered in *slg2* and *slg3* mutants in correlation with their carotenoid profile

Lines with reduced levels of plastidial GGPPS activity also showed changes in reproductive development (Fig. 7). Flowering time was similar in WT, *slg2* and *slg3* plants (Fig. 7a). However, pigmentation changes associated to fruit ripening were visually delayed in mutant fruits (Fig. 7b). Tomato fruits reach their final size at the mature green (MG) stage and then they start the ripening process. The first visual symptoms of ripening define the breaker (B) stage, when chlorophyll degradation and carotenoid biosynthesis change the fruit colour from green to yellow (Fig. 7c). As ripening advances, accumulation of orange and red carotenoids (β-carotene and lycopene, respectively) progressively change the fruit colour and define the orange (O) and eventually
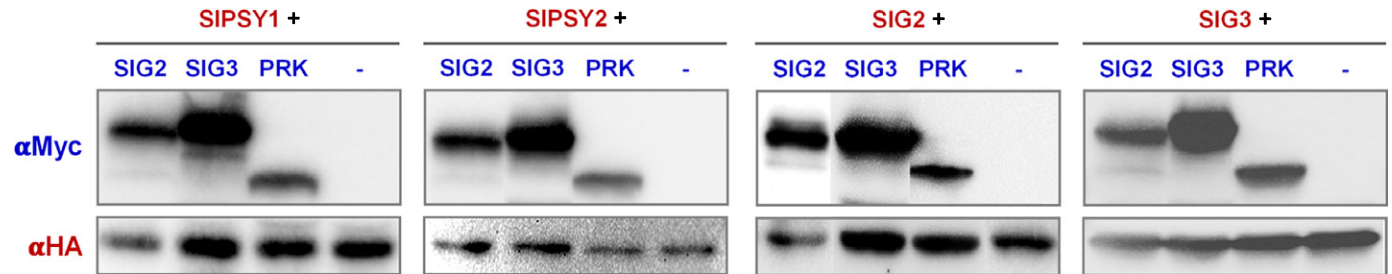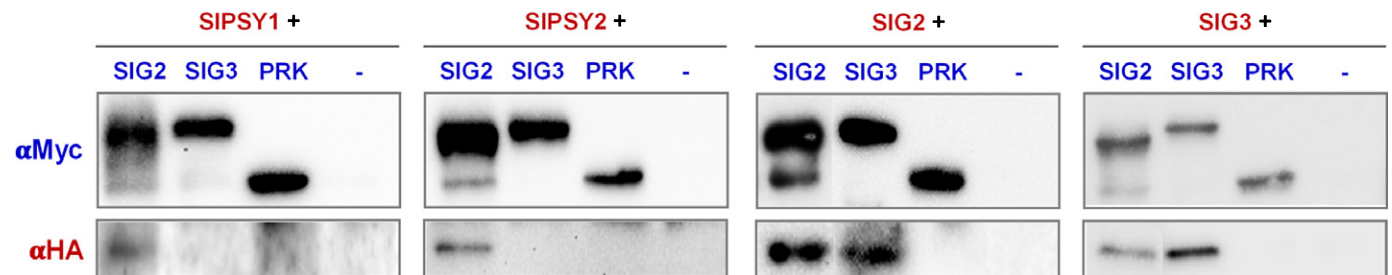
INPUT

IP (αMyc)

Fig. 3 Co-immunoprecipitation analyses. *Nicotiana benthamiana* leaves were co-agroinfiltrated with the indicated proteins tagged with C-terminal Myc (in blue) or HA (in red) epitopes. Controls agroinfiltrated only with the HA-tagged protein are indicated as (−). A fraction of the protein extracts (INPUT) was used to test protein production using immunoblot analyses using antibodies against Myc (αMyc) and HA (αHA). After immunoprecipitation (IP) of the remaining protein extracts using αMyc, samples were used for immunoblot analyses with αMyc (to confirm successful IP) and αHA (to detect the presence of co-immunoprecipitated HA-tagged proteins).

red (R) stages (Fig. 7c). The time from anthesis to B was similar in WT and SlG2-defective fruits, but it was longer in the *slg3* mutants (Figs 7b, S9). Fruits from lines defective in SlG3, but also those defective in SlG2, showed a pigmentation delay in the transition from B to O. The delay was observed both on vine (i.e. in fruits attached to the plant) and off vine (i.e. in fruits detached from the plant at the B stage; Figs 7b, S9). Both on-vine and off-vine measurements revealed that *slg2* mutants also took longer to reach the R stage compared with WT fruits (Fig. S9), whereas *slg3* mutants did not reach a proper R stage, as they developed a dark-orange colour when ripe and never turned fully red (Fig. 7c).

WT and mutant fruits showed similar levels of carotenoids, chlorophylls and tocopherols at the MG stage (Fig. S10), but clear differences were detected in ripe fruits at B + 10, i.e. 10 d after B (Figs 6, 7d; Table S7). Phytoene and lycopene were decreased in all mutants, although the effect was higher for *slg3* fruits. No significant differences were found for β-carotene, although the levels of this orange carotenoid tended to be higher in *slg3* mutants. This, together with the lower levels of the red carotenoid lycopene, may explain the dark-orange colour of B + 10 *slg3* fruits (Fig. 7c). Tocopherols also showed a trend towards higher abundance in SlG3-deficient fruits, a change that was statistically significant in the *slg3-1* allele (Fig. 7d) or when *slg3-1* and *slg3-2* samples were considered together (Fig. 6).

Unlike that observed in young leaves, ABA levels were reduced in B + 10 fruits of *slg2* and, most strongly, *slg3* mutants compared with WT controls (Fig. 6; Table 2). At the level of primary

metabolites, B + 10 fruits from both *slg2* and *slg3* mutants exhibited increased levels of raffinose, galacturonate, pyruvate and Asp and lower levels of Ser, Gly, Tyr, Val, Ala, Glu and GABA compared with WT controls (Fig. 6). The changes in these metabolites were typically stronger for *slg3* fruits, paralleling that observed for carotenoids and derived ABA levels.

Double mutants defective in both SlG2 and SlG3 are not viable

To assess the impact of simultaneous disruption of both *SlG2* and *SlG3* genes, alleles *slg2-2* and *slg3-1* were crossed using the former as female parent and the latter as male parent or *vice versa*. Double heterozygous F1 plants from each cross were allowed to self-pollinate and the resulting seeds were used to screen the F2 population for double homozygous plants, which were expected to occur at a Mendelian frequency of 6.25% (1 in 16). We performed two rounds of screening. In the first one, 200 seeds (100 from each cross) were plated and all of them germinated and produced green seedlings. In the second round, carried out with older seeds, 80 seeds were plated and 76 (95%) germinated (Table 3). The seeds that failed to germinate (four) were manually open and found to contain either albino/pale (three) or green (one) embryos (Fig. S11). PCR genotyping of these embryos (Fig. S11) and of the remaining 276 seedling did not identify double homozygous mutants (Table 3). A chi-squared goodness-of-fit test performed with 8 degrees of freedom and 95% interval of confidence confirmed that the observed genotype frequencies
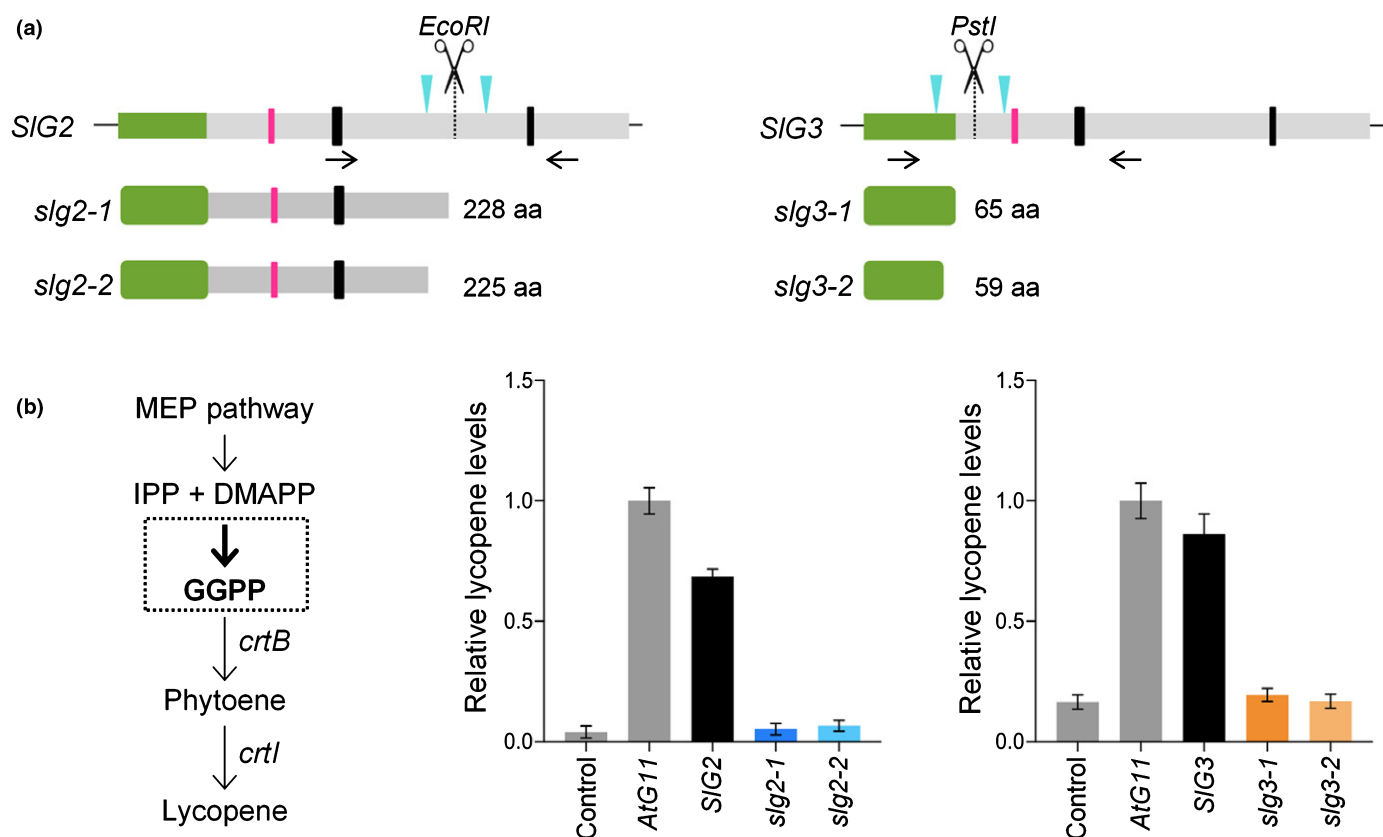
Fig. 4 CRISPR-Cas9 mutagenesis of tomato *SlG2* and *SlG3* genes. (a) Scheme representing the designed strategy to generate deletions on *SlG2* and *SlG3* genes and the resulting proteins in selected mutant alleles (see Supporting Information Figs S6–S8 for further details). Green, pink and black boxes represent transit peptides, protein–protein interaction motifs, and catalytic domains (FARM and SARM), respectively. Blue arrowheads indicate the position of the designed sgRNAs encompassing specific restriction sites, and black arrows represent primer pairs used for genotyping. (b) Activity assays of wild-type (WT) and mutant GGPPS enzymes in *E. coli* strains expressing bacterial genes for lycopene biosynthesis (*crtB* and *crtI*) but lacking GGPPS activity. Lycopene production after transformation with an empty vector (labelled as 'Control' in the plots) or plasmid constructs harbouring the indicated sequences is represented relative to the levels obtained with the true GGPPS enzyme AtG11. Values represent the mean ± SD of at least three independent transformants ($n = 3$).

did not follow the expected Mendelian segregation in any of the two experiments or when considering all data together (Table 3). In addition to the absence of double *slg2-2 slg3-1* mutants (here referred to as *g2g2 g3g3*), lines with one of the two genes in homozygosis and the second one in heterozygosis (i.e. *g2g2 G3g3* and *G2g2 g3g3*) were found at lower frequencies than predicted (Table 3), suggesting a gene dosage effect. Our interpretation of these results is that the absence of both *SlG2* and *SlG3* results in a lethal phenotype that is partially rescued by incorporating one copy of any of these two genes (as in *g2g2 G3g3* or *G2g2 g3g3* plants), and fully rescued when two copies are present in the genome (as in double heterozygous or single homozygous mutants). These results, together with the similar expression levels of both genes in developing tomato seeds (Fig. S4), suggest that SlG2 and SlG3 contribute similarly and additively to embryo or/and seed development.

The phenotypes of single *slg3* mutants are exacerbated in lines with the *SlG2* gene in heterozygosis

Plants segregating from double heterozygous F1 plants (*G2g2 G3g3*) that showed a single mutant genotype (i.e. *g2g2 G3G3*

and *G2G2 g3g3*) or one of the two genes in homozygosis and the second one in heterozygosis (i.e. *g2g2 G3g3* and *G2g2 g3g3*) were transferred to soil and used to carefully examine their phenotype. Consistent with that described for the *slg2-2* and *slg3-1* parentals (Fig. 5), young leaves of *g2g2 G3G3* plants showed unchanged pigmentation and WT levels of photosynthetic pigments (chlorophylls and carotenoids) and photosynthetic activity (ϕPSII), whereas those of *G2G2 g3g3* plants were paler and displayed a reduction of photosynthetic pigments and activity (Fig. 8). Most interestingly, the phenotypes of the *slg3* mutants were intensified when one of the two genomic copies of *SlG2* was inactivated in the *G2g2 g3g3* line (Fig. 8). Loss of an *SlG3* gene copy in the *slg2* mutant background, however, was not sufficient to trigger statistically significant changes in young leaves compared with WT or *slg2* lines. This result indicates that a single copy of the *SlG3* gene is sufficient to provide GGPP for the production of photosynthetic pigments in chloroplasts, even when no SlG2 activity is available. For mature leaves, no significant differences were observed between WT and any of the mutant lines (Fig. 8).

At the level of fruit ripening, quantification of fruit colour using the TomatoAnalyzer 4.0 tool (Gonzalo *et al.*, 2009) confirmed the pigmentation delay previously observed in single mutants defective
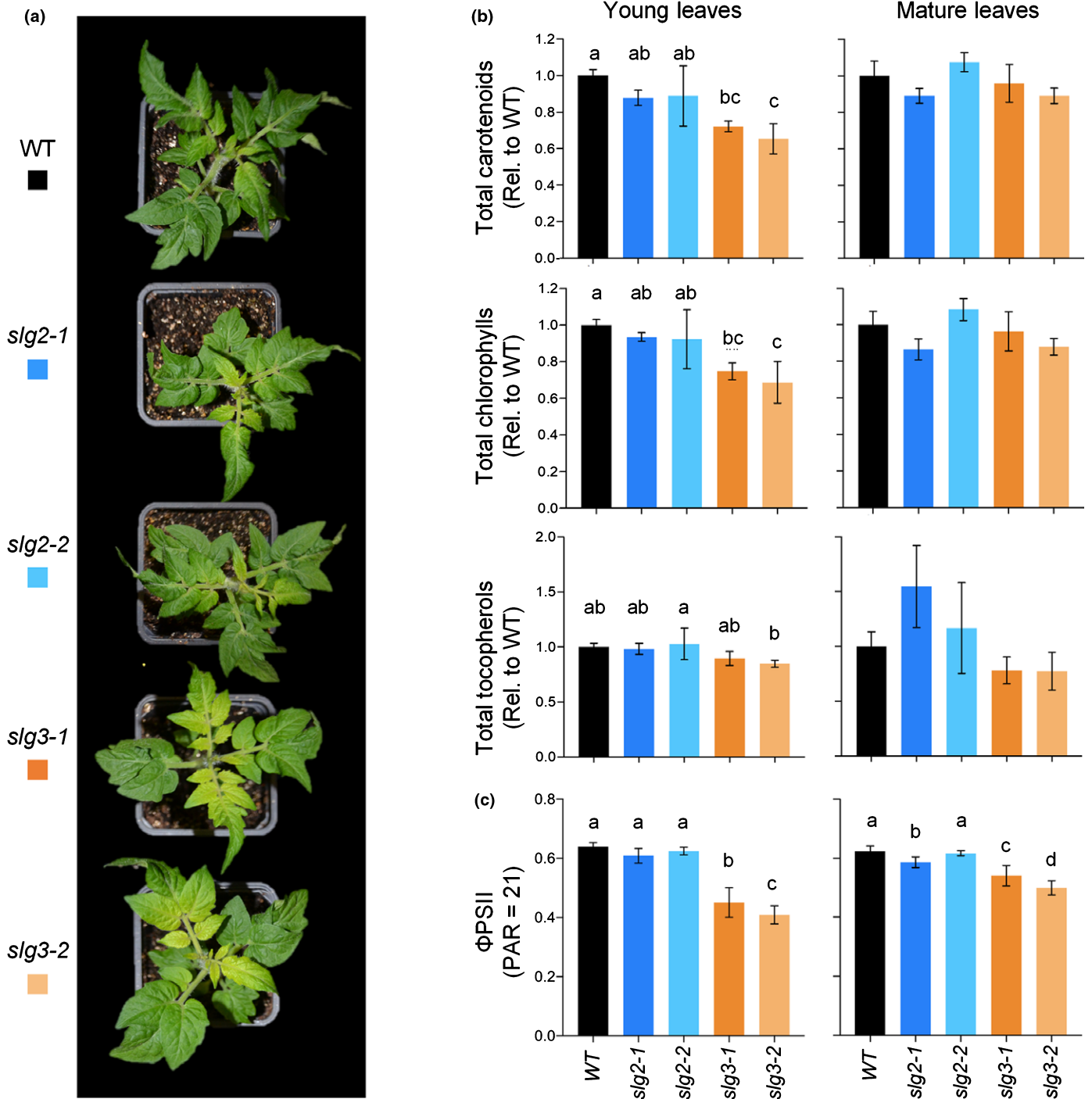
Fig. 5 Leaf phenotypes of mutant tomato lines defective in SlG2 or SlG3. (a) Representative images of 4-wk-old plants of the indicated lines. (b) Relative levels of total carotenoids, chlorophylls and tocopherols in young and mature leaves of wild-type (WT) and mutant lines. Values are represented relative to WT levels and they correspond to the mean ± SD of at least three independent biological replicates ($n = 3$). See Supporting Information Table S7 for absolute values. (c) ϕPSII in young and mature leaves of the indicated lines. Values represent the mean ± SD of four different leaf areas from three different plants. In all cases, different letters represent statistically significant differences ($P < 0.05$) among means according to post hoc Tukey's tests run when one-way ANOVA detected different means.

in SlG2 or, to a higher extent, SlG3 (Fig. 7) and further showed a stronger effect when one of the two genomic copies of *SlG2* was additionally inactivated in the *slg3* background (Fig. 9a). Analysis of the expression of ripening marker genes such as *E8* and *ACS2* (Estornell *et al.*, 2009; Llorente *et al.*, 2016; D'Andrea *et al.*, 2018)

showed that the peak of *E8* and *ACS2* expression observed at the onset of ripening (Fig. S4) was reduced in the mutants (Fig. 9b). Again, the stronger effect was observed in lines without SlG3 activity and tended to be higher in *G2g2 g3g3* compared with *G2G2 g3g3* lines (Fig. 9b).

Fig. 6 Metabolic changes in *slg2* and *slg3* mutants. Colours represent statistically significant fold-change (FC) values (*t*-test, $P < 0.05$) of metabolite levels in young leaves or ripe fruit (B + 10) from mutant tomato plants relative to those in wild-type (WT) controls. Quantitative and technical data are detailed in Supporting Information Tables S8 and S9 for leaves and Tables S10 and S11 for fruit.

Table 2 ABA levels in GGPPS-defective tomato leaves and fruit.

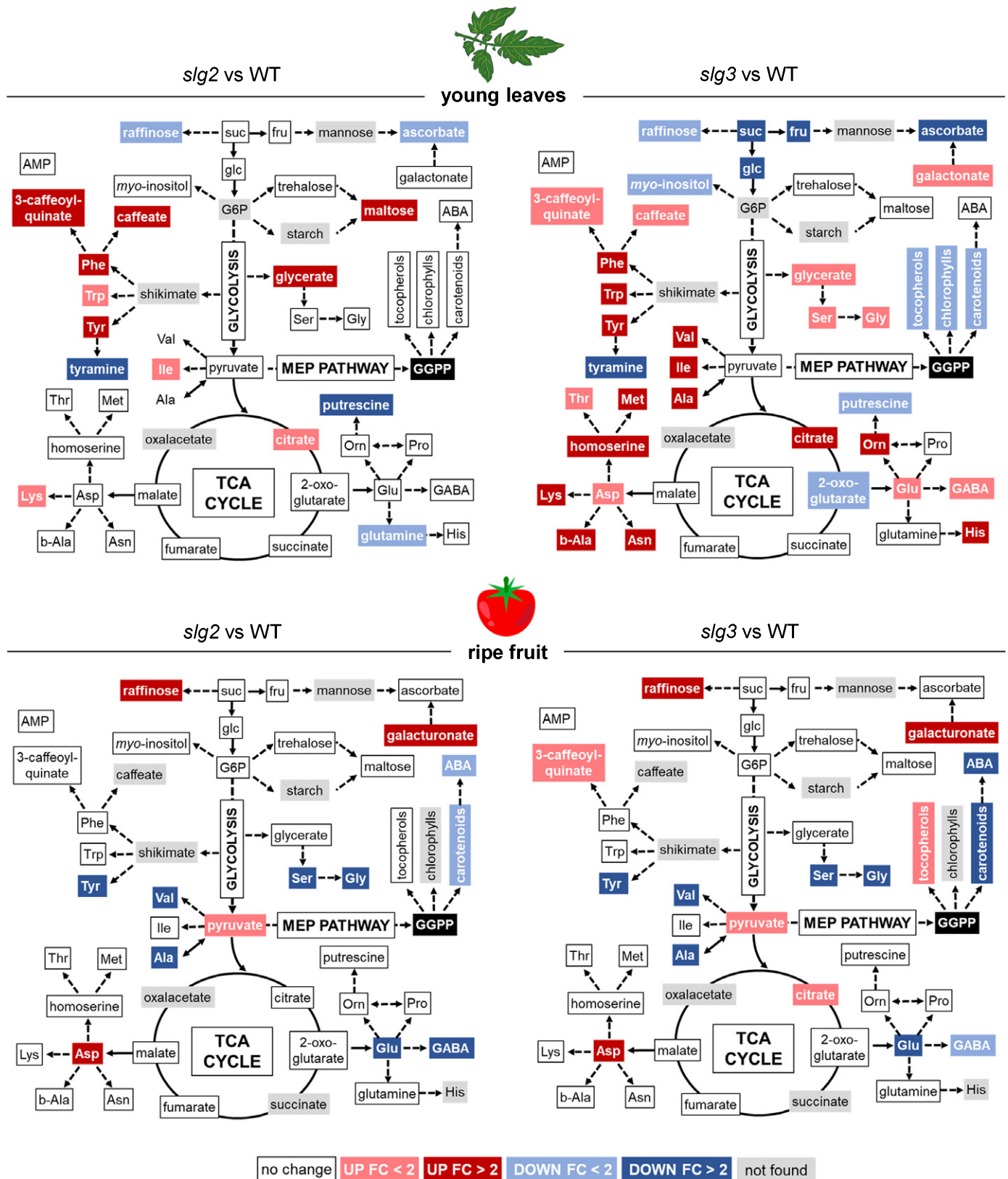|	Young leaves	B + 10 fruit
WT	1.67 ± 0.19	0.63 ± 0.13
slg2-1	1.69 ± 0.10	0.55 ± 0.12
slg2-2	1.98 ± 0.39	**0.30 ± 0.08**
slg3-1	1.96 ± 0.09	**0.16 ± 0.04**
slg3-2	1.61 ± 0.29	**0.08 ± 0.01**

Values ($\mu g\ g^{-1}$ dry weight) correspond to the mean ± SD of four independent samples ($n = 4$). Statistically significant changes in mutants compared with wild-type (WT) samples (t-test, $P < 0.01$) are indicated in bold.

Discussion

The fundamental basis for our knowledge of the regulation of GGPP biosynthesis in plants mainly comes from the characterisation of the Arabidopsis GGPPS family (Zhu *et al.*, 1997a,b; Okada *et al.*, 2000; Beck *et al.*, 2013; Nagel *et al.*, 2015; Wang *et al.*, 2016; Ruiz-Sola *et al.*, 2016a,b). In this model plant, there are two plastid-targeted GGPPS paralogues (AtG2 and AtG11) but only AtG11 appears to be required for the production of plastidial isoprenoids (Beck *et al.*, 2013; Nagel *et al.*, 2015; Ruiz-Sola *et al.*, 2016a,b). The gene encoding AtG11 is ubiquitously expressed at high levels and can generate long transcripts encoding the plastid-targeted isoform, but also short transcripts encoding a cytosolic enzyme that retains enzymatic activity and is essential for embryo development (Ruiz-Sola *et al.*, 2016a). The production of GGPP has also been studied in a few crop plants (Wang & Dixon, 2009; Zhang *et al.*, 2015; Zhou *et al.*, 2017; Wang *et al.*, 2018, 2019). Similar to Arabidopsis, rice and pepper contain only one enzymatically active GGPPS isoform localised in plastids, named OsGGPPS1 (OsG1 in short) and CaGGPPS1 (CaG1), respectively (Zhou *et al.*, 2017; Wang *et al.*, 2018). Strikingly, only scattered information has been available to date on the tomato GGPPS family, despite this species being a well established model plant that accumulates high amounts of GGPP-derived metabolites of human interest such as carotenoids in fruits. Here we demonstrate that, in tomato, two plastidial isoforms (SlG2 and SlG3) co-ordinately supply GGPP to produce carotenoids and other isoprenoids essential for photosynthesis, fruit pigmentation and seed viability.

Subfunctionalisation of plastidial GGPPS paralogues in tomato might involve several mechanisms with a major role for differential gene expression

The three plastid-targeted GGPPS homologues present in tomato (SlG1-3) produce GGPP with similar kinetic parameters and an optimal pH around 7.5 (Fig. S3; Table 1). Several mechanisms might allow enzymatically similar GGPPS isoforms to acquire new functions, including: (a) localisation in distinct subcellular compartments, (b) specific interactions with other protein, and (c) diversification of spatio-temporal gene expression patterns. Despite the clear plastidial localisation observed here (Fig. S1) and elsewhere (Zhou & Pichersky, 2020) for GFP

fusions of the SlG1-3 isoforms, we cannot exclude the possibility that shorter extraplastidial versions of these proteins could also be produced *in vivo*, paralleling that observed for AtG11 (Ruiz-Sola *et al.*, 2016a). Indeed, several M residues can be found in the N-terminal region of both SlG2 and SlG3 enzymes (Fig. S8); they could be used as alternative translation start sites to produce catalytically active GGPPS enzymes with an absent or shorter (i.e. dysfunctional) plastid-targeting domain.

In addition to localisation in distinct subcellular compartments, subfunctionalisation of GGPPS paralogues might also involve isoform-specific interactions with other proteins. The enzymatic properties of GGPPS proteins change to produce GPP upon heterodimerisation with members of the GPP synthase small subunit type I (SSU-I) subfamily (Orlova *et al.*, 2009; Wang & Dixon, 2009). This occurs upon interaction of SlG1-3 enzymes with the tomato SSU-I protein (Solyc07g064660; Zhou & Pichersky, 2020). Multienzymatic complexes appear to be particularly important for metabolic channelling of GGPP. In particular, PSY cannot access freely diffusible GGPP or time-displaced GGPP supply by GGPPS (Camagna *et al.*, 2019). Arabidopsis AtG11 and pepper CaG1 can directly interact with PSY proteins (Ruiz-Sola *et al.*, 2016b; Wang *et al.*, 2018; Camagna *et al.*, 2019). We found that tomato SlG2, but not SlG3, is able to interact with PSY1 and PSY2 *in planta* (Fig. 3). However, tomato SlG3 might deliver GGPP to PSY enzymes by heterodimerisation with PSY-interacting SlG2 (Fig. 3). An alternative possibility involves interaction with members of another catalytically inactive SSU subfamily, named type II (SSU-II). Similar to AtG11 and CaG1, OsG1 is the only GGPPS enzyme producing GGPP for carotenoid biosynthesis in rice. Strikingly, OsG1 does not interact with PSY, but heterodimerises with a SSU-II homologue, resulting in its delivery to a large protein complex in thylakoid membranes (Zhou *et al.*, 2017). The interaction with SSU-II proteins was also shown to enhance not only the GGPP-producing activity of rice OsG1 but also of pepper CaG1 (Wang *et al.*, 2018) and tomato SlG1-3 isoforms (Zhou & Pichersky, 2020). Interestingly, the pepper SSU-II protein also interacts with PSY, suggesting that binding of CaG1 to SSU-II might stimulate both its GGPPS activity and its interaction with PSY (Wang *et al.*, 2018). It is therefore possible that heterodimerisation with tomato SSU-II (Solyc09g008920) might also deliver SlG3 to PSY-containing protein complexes and enhance interaction of SlG2 with PSY isoforms.

Regardless of other possible mechanisms discussed above, it appears that a major determinant defining the biological roles of plastidial GGPPS isoforms in tomato is their distinct expression profiles. Mining of public tomato gene expression databases, GCN analyses and qPCR assays led us to conclude that SlG1 is likely to contribute to carotenoid biosynthesis in roots together with PSY3. This conclusion is supported by a recent study showing that the expression of *PSY3* and *SlG1* co-ordinately responds to tomato root mycorrhization and phosphate starvation (Stauder *et al.*, 2018). The SlG1–PSY3 tandem might be channelling the flux of MEP-derived precursors towards the synthesis of carotenoid-derived molecules, such as strigolactones and apocarotenoids, that are crucial for the establishment of symbiosis
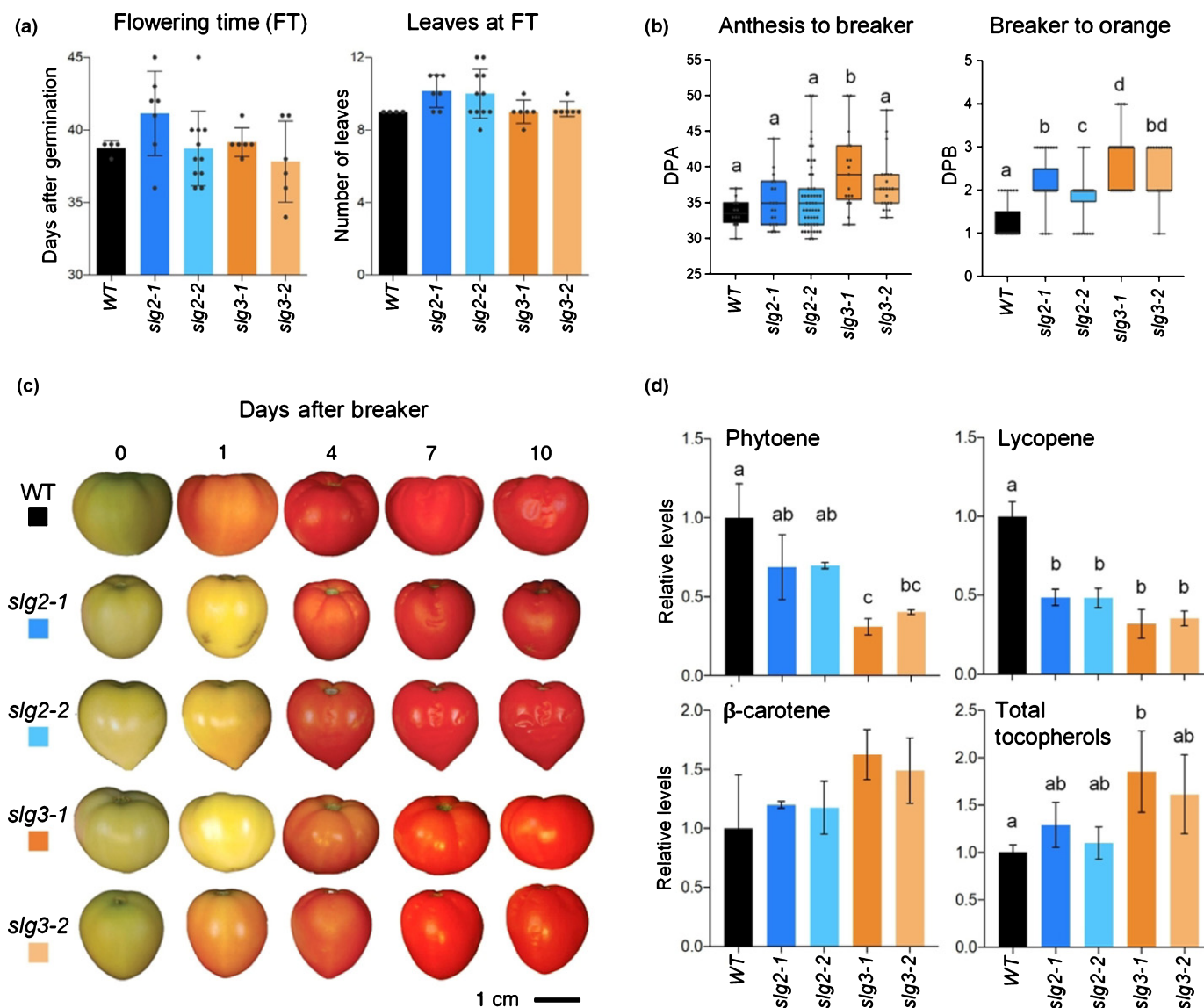
Fig. 7 Flowering and fruit phenotypes of mutant tomato lines defective in SlG2 or SlG3. (a) Flowering time measured as days after germination (left) or number of leaves (right). Values correspond to the mean ± SD of at least $n = 4$ independent biological replicates. (b) Number of days to reach the indicated ripening stages represented as days post anthesis on vine (DPA, left) and days post breaker off vine (DPB, right). In both box-plots, the lower boundary of the boxes indicates the 25th percentile, the black line within the boxes marks the median, and the upper boundary of the boxes indicates the 75th percentile. Dots mark data values and whiskers above and below the boxes indicate the minimum and maximum values. (c) Representative images of fruit from WT and mutant lines harvested from the plant at the breaker stage. (d) Relative levels of individual carotenoids (phytoene, lycopene and β-carotene) and total tocopherols in fruits of wild-type (WT) and mutant linesat the B+10 stage. Values are represented relative to those in WT samples and correspond to the mean ± SD of $n = 3$ independent biological replicates. See Supporting Information Table S7 for absolute values. In all plots, different letters represent statistically significant differences (one-way ANOVA followed by Tukey's multiple comparisons test, $P < 0.05$).

(Stauder *et al.*, 2018). Unlike *SlG1*, *SlG2* and *SlG3* are constitutively expressed, with *SlG3* being the paralogue with the highest expression level in all plant tissues (Fig. S4). In leaves, *SlG2* is more strongly co-expressed than *SlG3* with genes from photosynthesis-related isoprenoid pathways (Fig. 1). This suggests that the expression of the *SlG2* gene changes more than that of *SlG3* to adapt to conditions requiring a re-adjustment of the gene expression network regulating the metabolism of isoprenoids such as carotenoids. In agreement, *SlG2* was much more upregulated than *SlG3* during seedling de-etiolation (Fig. 2) and leaf

development (Fig. S4c), in which an enhanced production of carotenoids and other photosynthesis-related isoprenoids contributes to assemble a functional photosynthetic machinery. *SlG2* was also much more induced than *SlG3* during fruit ripening, when carotenoid biosynthesis is boosted thanks to the upregulation of the PSY1 isoform. *PSY1* and *SlG2*, but not *SlG3*, are coordinately regulated by FUL and RIN transcription factors that control the expression of ripening-related genes, including many of the MEP and carotenoid pathway genes (Fujisawa *et al.*, 2013, 2014).

Table 3 Expected and observed frequencies of the F2 population from the crosses of *slg2-2* and *slg3-1* mutant tomato plants.

Genotypes	Expected (%)	Round 1		Round 2		Combined	
		n	%	n	%	n	%
G2*g2* G3*g3*	25	52	26	15	20	67	24
G2*g2* G3G3	12.5	26	13	18	24	44	16
G2G2 G3*g3*	12.5	35	17.5	10	13	45	16
g2g2 G3*g3*	12.5	18	9	6	8	24	9
G2*g2* *g3g3*	12.5	16	8	5	7	21	8
g2g2 *g3g3*	6.25	0	0	0	0	0	0
g2g2 G3G3	6.25	17	8.5	5	7	22	8
G2G2 *g3g3*	6.25	14	7	8	11	22	8
G2G2 G3G3	6.25	22	11	9	12	31	11
Total plants (n)		200		76		276	
Chi-square			30.84		22.68		45.17
P-value			0.0002		0.0038		< 0.0001

Mutant alleles are marked in red. A chi-squared goodness-of-fit test was performed with 8 degrees of freedom and 95% confidence interval to check the Mendelian segregation of the mutant alleles. *n*, number of plants.

All these expression data showed that *SlG2* expression is more responsive to sudden demands of precursors for the production of isoprenoids, including carotenoids. By contrast, *SlG3* expression is higher and does not change as much, suggesting a housekeeping role to maintain a continuous supply of GGPP in plastids for basal production of carotenoids and other isoprenoids. According to this model, SlG1 and SlG2 would help SlG3 to supply GGPP when a boost in carotenoid production is needed. The very low and restricted expression level of *SlG1*, however, strongly suggests that SlG2 is the main helper isoform for SlG3 in chloroplasts of cotyledons and expanding leaves and chromoplasts of ripening fruit.

GGPPS isoforms SlG2 and SlG3 have functionally interchangeable roles in chloroplasts and chromoplasts

Analysis of tomato mutants defective in gene copies for SlG2 or/and SlG3 further suggested that these are functionally exchangeable isoforms that participate in the same biological processes. This might not be obvious when analysing leaves, as only *slg3* alleles were found to display reduced levels of GGPP-derived isoprenoids and subsequent inhibition of photosynthesis (Figs 5, 8). However, the effects of reduced isoprenoid synthesis could also be indirectly detected in *slg2* leaves. Our GC-MS analysis showed higher levels of all aromatic amino acids derived from the shikimate pathway (Trp, Tyr and Phe) as well as Phe-derived phenylpropanoids caffeate (caffeic acid) and 3-caffeoyl-quinate (chlorogenic acid) in both *slg2* and *slg3* mutant lines (Fig. 6). This might be a physiological response to cope with photo-oxidative stress caused by lower levels of carotenoids in the mutants, as phenylpropanoids (including Phe-derived flavonoids and anthocyanins) can also function as photoprotective metabolites (Muñoz & Munné-Bosch, 2018). Reduced levels of well known metabolites associated with oxidative stress such as ascorbate and putrescine in leaves from both mutant lines would also support this view.

Loss of one *SlG3* gene copy in the *slg2* mutant background failed to cause a statistically significant decrease in the levels of photosynthetic pigments or activity, even though a trend towards reduction of chlorophyll and carotenoid levels was observed (Fig. 8). However, complete loss of SlG3 activity in lines with one or two functional *SlG2* copies was sufficient to reduce levels of GGPP-derived photoprotective isoprenoids such as carotenoids and tocopherols to an extent that became detectable and affected photosynthesis (Fig. 5), causing sugar starvation and the subsequent metabolic changes observed only in the *slg3* mutant (Fig. 6). In agreement, the increased accumulation of most amino acids in *slg3* leaves suggested a high proteolytic activity to generate an alternative respiratory source, a probable response to sugar starvation derived from reduced photosynthesis and/or photo-oxidative stress (Araújo *et al.*, 2011; Obata & Fernie, 2012; Galili *et al.*, 2016).

The absence of any of the two individual enzymes also decreases plastidial GGPP production in fruit, as deduced from the levels of the main GGPP-derived metabolites (Fig. 7d; Table S7). Tocopherol levels did not decrease in mutant fruit, perhaps because they are mostly produced by recycling the phytyl chain released from the chlorophylls degraded during fruit ripening. By contrast, lycopene (by far the most abundant carotenoid in ripe fruit) and, to a lower extent, phytoene, showed reduced levels in both mutants (Fig. 7d; Table S7). Similar to that observed in leaves, the effect is stronger in *slg3* mutants, consistent with the higher expression levels of the *SlG3* compared with *SlG2* in young leaves and MG fruits (Fig. S4). While altered levels of 3-caffeoyl-quinate and citrate were detected only in fruit of the *slg3* mutant, the rest of the metabolic changes were similar in *slg2* and *slg3* lines (Fig. 6), again supporting the conclusion that these enzymes are redundant and interchangeable. In particular, both *slg2* and *slg3* fruit showed pigmentation defects that were associated with a decreased carotenoid accumulation (Figs 7, 9a). Because ABA is synthesised from carotenoids, its reduced levels in GGPPS-defective ripe fruits, but not in leaves (Table 2),
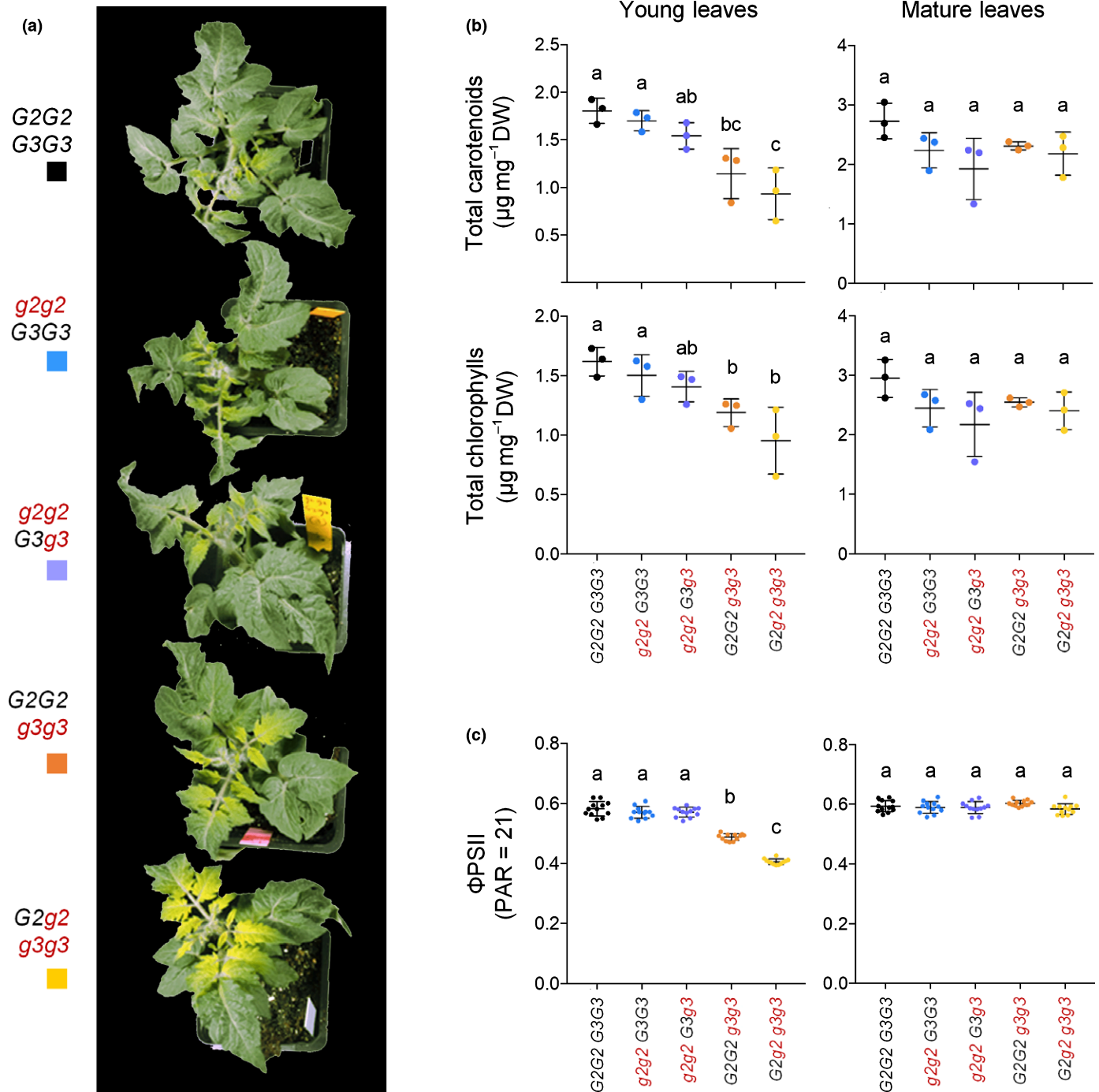
Fig. 8 Leaf phenotypes of tomato lines with different combinations of *slg2* and *slg3* mutations. (a) Representative images of 4-wk-old plants of the indicated lines. Mutant alleles are marked in red. (b) Total levels of photosynthetic pigments (carotenoids and chlorophylls) in young and mature leaves of wild-type (WT) and mutant lines. Values, mean and SD of $n = 3$ independent biological replicates are represented. (c) ϕPSII in young and mature leaves of the indicated lines. Values, mean and SD of four different leaf areas from three different plants are shown. In all plots, different letters represent statistically significant differences ($P < 0.05$) among means according to post hoc Tukey tests that were run once the existence of different means was established using one-way ANOVA.

may be the result of a more substantial reduction in carotenoid contents in mutant fruit (Fig. 7) compared with leaves (Fig. 5; Table S7). A role for ABA in promoting tomato fruit ripening has been proposed based on the analysis of mutants or external application of hormones and inhibitors. This, together with the observed downregulation of ethylene-related ripening marker genes (*E8* and *ACS2*) in GGPPS-defective fruit (Fig. 9b), allowed us to speculate that reduced ABA levels in the mutant fruit may contribute to a delay in ripening, either directly or indirectly by ethylene (Zhang *et al.*, 2009; McQuinn *et al.*, 2020).
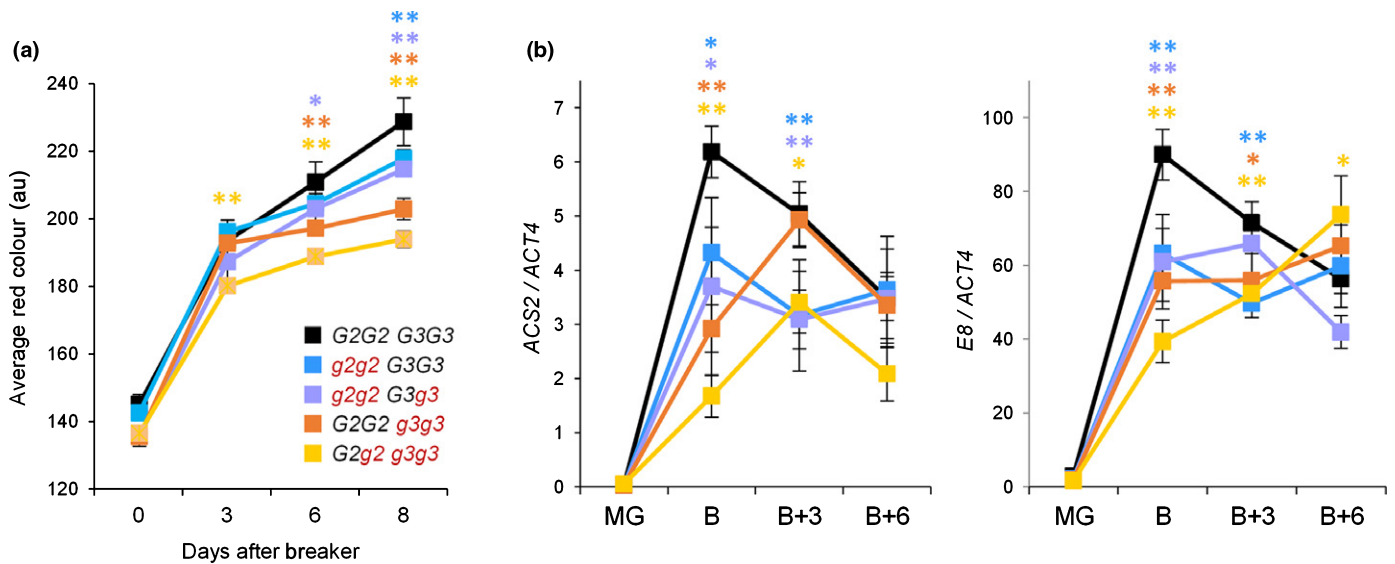
Fig. 9 Ripening-associated pigmentation and marker gene expression in tomato fruits with different combinations of *slg2* and *slg3* mutations. (a) Average red colour quantification (arbitrary units) of on-vine fruit from wild-type (WT) and mutant lines at the indicated times. Values represent the mean ± SD of three different fruits (*n* = 3) for each point. (b) RT-qPCR analysis of *ACS2* and *E8* transcript levels in WT and mutant fruits collected at the indicated developmental stages. Expression values were normalised using *ACT4* and represent the mean ± SD of *n* = 3 independent biological replicates. In all plots, asterisks indicate statistically significant differences among means relative to WT samples (*t*-test: *, $P < 0.05$; **, $P < 0.01$). Asterisk colour represents the genotype.

Additionally, metabolic roles of SlG2 and SlG3 in addition to their GGPPS activity in plastids might play a role in fruits but also in developing seeds, therefore explaining why we could not isolate a double *slg2 slg3* mutant (Table 3). The observation that the lethal phenotype is dose dependent in an isoform-independent fashion (i.e. can be rescued by a single genomic copy of either *SlG2* or *SlG3*) reinforces our conclusion that SlG2 and SlG3 have functionally interchangeable roles.

Concluding remarks

Retention of multiple gene copies after duplication events may allow the acquisition of new functions (neofunctionalisation) or partitioning the ancestral functions between duplicate partners (subfunctionalisation), by evolution of coding sequence and/or regulatory regions. The work reported here demonstrates that the bulk of GGPP production in tomato leaf chloroplasts and fruit chromoplasts relies on two redundant, but cooperating, GGPPS paralogues, SlG2 and SlG3. Additionally, the SlG1 isoform might contribute to GGPP synthesis in root plastids. This subfunctionalisation scenario contrasts with that described to date in other plant species such as Arabidopsis, rice or pepper, which produce their essential plastidial isoprenoids using a single GGPPS isoform. However, it is likely that tomato is not an exception. Examples of gene families encoding enzyme isoforms located in the same cell compartment, but differing in gene expression profiles abound in the literature. They include deoxyxylulose 5-phosphate synthase (DXS) and PSY, the rate-determining enzymes of the MEP and carotenoid pathways, respectively (Walter *et al.*, 2015). Both DXS and PSY are encoded by single genes in Arabidopsis, but several differentially expressed genes in tomato. Subfunctionalisation is also widespread beyond

the isoprenoid pathway, contributing to the huge diversity of specialised metabolism in plants (Moghe & Last, 2015). Deciphering how different plants regulate plastidial GGPP production and channelling will be useful for future metabolic engineering approaches targeted to manipulate the accumulation of specific groups of GGPP-derived isoprenoids without negatively impacting the levels of others.

Author contributions

MVB, ME and MRC designed the research; MVB, ME, SB, GD, IFS, EF and AF performed research; RK, ARF and JB contributed analytic tools; MVB, ME, SB, GD, IFS, EF, AF, RK, ARF, JB and MRC analysed data; MVB and MRC wrote the paper. MVB and ME contributed equally to this work.

ORCID

M. Victoria Barja (ID) https://orcid.org/0000-0002-3846-4885
Jules Beekwilder (ID) https://orcid.org/0000-0003-3238-4427
Gianfranco Diretto (ID) https://orcid.org/0000-0002-1441-0233
Miguel Ezquerro (ID) https://orcid.org/0000-0002-3051-5502
Elisenda Feixes (ID) https://orcid.org/0000-0003-0285-1979
Alisdair R. Fernie (ID) https://orcid.org/0000-0001-9000-335X
Igor Florez-Sarasa (ID) https://orcid.org/0000-0002-1862-7931
Rumyana Karlova (ID) https://orcid.org/0000-0003-0230-6428
Manuel Rodríguez-Concepción (ID) https://orcid.org/0000-0002-1280-2305

REFERENCES

Ahrazem O, Argandoña J, Fiore A, Aguado C, Luján R, Rubio-Moraga Á, Marro M, Araujo-Andrade C, Loza-Alvarez P, Diretto G *et al.* **2018.** Transcriptome analysis in tissue sectors with contrasting crocins accumulation provides novel insights into apocarotenoid biosynthesis and regulation during chromoplast biogenesis. *Scientific Reports* **8**: 1–17.

Ament K, Van Schie CC, Bouwmeester HJ, Haring MA, Schuurink RC. 2006. Induction of a leaf specific geranylgeranyl pyrophosphate synthase and emission of (E,E)-4,8,12-trimethyltrideca-1,3,7,11-tetraene in tomato are dependent on both jasmonic acid and salicylic acid signaling pathways. *Planta* **224**: 1197–1208.

Araújo WL, Tohge T, Ishizaki K, Leaver CJ, Fernie AR. 2011. Protein degradation – an alternative respiratory substrate for stressed plants. *Trends in Plant Science* **16**: 489–498.

Barja MV, Rodríguez-Concepción M. 2020. A simple *in vitro* assay to measure the activity of geranylgeranyl diphosphate synthase and other short-chain prenyltransferases. *Methods in Molecular Biology* **2083**: 27–38.

Bartley G, Scolnik P. 1993. cDNA cloning, expression during development, and genome mapping of a second phytoenen synthase. *Biochemistry* **268**: 25718–25721.

Bartley GE, Viitanen PV, Bacot KO, Scolnik PA. 1992. A tomato gene expressed during fruit ripening encodes an enzyme of the carotenoid biosynthesis pathway. *Journal of Biological Chemistry* **267**: 5036–5039.

Baslam M, Esteban R, García-Plazaola JI, Goicoechea N. 2013. Effectiveness of arbuscular mycorrhizal fungi (AMF) for inducing the accumulation of major carotenoids, chlorophylls and tocopherol in green and red leaf lettuces. *Applied Microbiology and Biotechnology* **97**: 3119–3128.

Beck G, Coman D, Herren E, Ruiz-Sola MA, Rodríguez-Concepción M, Gruissem W, Vranová E. 2013. Characterization of the GGPP synthase gene family in *Arabidopsis thaliana*. *Plant Molecular Biology* **82**: 393–416.

Bradford MM. 1976. A rapid and sensitive method for the quantitation of microgram quantities of protein utilizing the principle of protein-dye binding. *Analytical Biochemistry* **72**: 248–254.

Camagna M, Grundmann A, Bär C, Koschmieder J, Beyer P, Welsch R. 2019. Enzyme fusion removes competition for geranylgeranyl diphosphate in carotenogenesis. *Plant Physiology* **179**: 1013–1027.

Camara B. 1993. Plant phytoene synthase complex: component enzymes, immunology and biogenesis. *Methods in Enzymology* **214**: 352–365.

D'Andrea L, Simon-Moya M, Llorente B, Llamas E, Marro M, Loza-Alvarez P, Li L, Rodriguez-Concepcion M. 2018. Interference with Clp protease impairs carotenoid accumulation during tomato fruit ripening. *Journal of Experimental Botany* **69**: 1557–1568.

Diretto G, Frusciante S, Fabbri C, Schauer N, Busta L, Wang Z, Matas AJ, Fiore A, Rose JKC, Fernie AR *et al.* **2020.** Manipulation of β-carotene levels in tomato fruits results in increased ABA content and extended shelf life. *Plant Biotechnology Journal* **18**: 1185–1199.

Dogbo O, Camara B. 1987. Purification of isopentenyl pyrophosphate isomerase and geranylgeranyl pyrophosphate synthase from *Capsicum* chromoplasts by affinity chromatography. *Biochimica et Biophysica Acta (BBA)/Lipids and Lipid Metabolism* **920**: 140–148.

Estornell LH, Orzáez D, López-Peña L, Pineda B, Antón MT, Moreno V, Granell A. 2009. A multisite gateway-based toolkit for targeted gene expression and hairpin RNA silencing in tomato fruits. *Plant Biotechnology Journal* **7**: 298–309.

Fernandez AI, Viron N, Alhagdow M, Karimi M, Jones M, Amsellem Z, Sicard A, Czerednik A, Angenent G, Grierson D *et al.* **2009.** Flexible tools for gene expression and silencing in tomato. *Plant Physiology* **151**: 1729–1740.

Fester T, Schmidt D, Lohse S, Walter MH, Giuliano G, Bramley PM, Fraser PD, Hause B, Strack D. 2002. Stimulation of carotenoid metabolism in arbuscular mycorrhizal roots. *Planta* **216**: 148–154.

Fester T, Wray V, Nimtz M, Strack D. 2005. Is stimulation of carotenoid biosynthesis in arbuscular mycorrhizal roots a general phenomenon? *Phytochemistry* **66**: 1781–1786.

Fraser PD, Enfissi EMA, Halket JM, Truesdale MR, Yu D, Gerrish C, Bramley PM. 2007. Manipulation of phytoene levels in tomato fruit: effects on isoprenoids, plastids, and intermediary metabolism. *Plant Cell* **19**: 3194–3211.

Fraser PD, Romer S, Shipton CA, Mills PB, Kiano JW, Misawa N, Drake RG, Schuch W, Bramley PM. 2002. Evaluation of transgenic tomato plants expressing an additional phytoene synthase in a fruit-specific manner. *Proceedings of the National Academy of Sciences, USA* **99**: 1092–1097.

Fraser PD, Schuch W, Bramley PM. 2000. Phytoene synthase from tomato (*Lycopersicon esculentum*) chloroplasts – partial purification and biochemical properties. *Planta* **211**: 361–369.

Fray RG, Grierson D. 1993. Identification and genetic analysis of normal and mutant phytoene synthase genes of tomato by sequencing, complementation and co-suppression. *Plant Molecular Biology* **22**: 589–602.

Fujisawa M, Nakano T, Shima Y, Ito Y. 2013. A large-scale identification of direct targets of the tomato MADS box transcription factor RIPENING INHIBITOR reveals the regulation of fruit ripening. *Plant Cell* **25**: 371–386.

Fujisawa M, Shima Y, Nakagawa H, Kitagawa M, Kimbara J, Nakano T, Kasumi T, Ito Y. 2014. Transcriptional regulation of fruit ripening by tomato FRUITFULL homologs and associated MADS box proteins. *Plant Cell* **26**: 89–101.

Galili G, Amir R, Fernie AR. 2016. The regulation of essential amino acid synthesis and accumulation in plants. *Annual Review of Plant Biology* **67**: 153–178.

Giorio G, Stigliani AL, D'Ambrosio C. 2008. Phytoene synthase genes in tomato (*Solanum lycopersicum* L.) - new data on the structures, the deduced amino acid sequences and the expression patterns. *FEBS Journal* **275**: 527–535.

Gonzalo MJ, Brewer MT, Anderson C, Sullivan D, Gray S, Van Der Knaap E. 2009. Tomato fruit shape analysis using morphometric and morphology attributes implemented in tomato analyzer software program. *Journal of the American Society for Horticultural Science* **134**: 77–87.

Goytia E, Fernández-Calvino L, Martínez-García B, López-Abella D, López-Moya JJ. 2006. Production of plum pox virus HC-Pro functionally active for aphid transmission in a transient-expression system. *Journal of General Virology* **87**: 3413–3423.

Höhner R, Aboukila A, Kunz H-H, Venema K. 2016. Proton gradients and proton-dependent transport processes in the chloroplast. *Frontiers in Plant Science* **7**: 1–7.

Kachanovsky DE, Filler S, Isaacson T, Hirschberg J. 2012. Epistasis in tomato color mutations involves regulation of phytoene synthase 1 expression by *cis*-carotenoids. *Proceedings of the National Academy of Sciences, USA* **109**: 19021–19026.

Liu H, Ding Y, Zhou Y, Jin W, Xie K, Chen LL. 2017. CRISPR-P 2.0: an improved CRISPR-Cas9 tool for genome editing in plants. *Molecular Plant* **10**: 530–532.

Llorente B, D'Andrea L, Ruiz-Sola MA, Botterweg E, Pulido P, Andilla J, Loza-Alvarez P, Rodriguez-Concepcion M. 2016. Tomato fruit carotenoid biosynthesis is adjusted to actual ripening progression by a light-dependent mechanism. *The Plant Journal* 85: 107–119.

Llorente B, Torres-Montilla S, Morelli L, Florez-Sarasa I, Matus JT, Ezquerro M, D'Andrea L, Houhou F, Majer E, Picó B *et al.* 2020. Synthetic conversion of leaf chloroplasts into carotenoid-rich plastids reveals mechanistic basis of natural chromoplast development. *Proceedings of the National Academy of Sciences, USA* 117: 21796–21803.

Maudinas B, Bucholtz ML, Papastephanou C, Katiyar SS, Briedis AV, Porter JW. 1977. The partial purification and properties of a phytoene synthesizing enzyme system. *Archives of Biochemistry and Biophysics* 180: 354–362.

McQuinn RP, Gapper NE, Gray AG, Zhong S, Tohge T, Fei Z, Fernie AR, Giovannoni JJ. 2020. Manipulation of ZDS in tomato exposes carotenoid- and ABA-specific effects on fruit development and ripening. *Plant Biotechnology Journal* 18: 2210–2224.

Moghe GD, Last RL. 2015. Something old, something new: conserved enzymes and the evolution of novelty in plant specialized metabolism. *Plant Physiology* 169: 1512–1523.

Muñoz A, Castellano MM. 2018. Coimmunoprecipitation of interacting proteins in plants. *Methods in Molecular Biology* 1794: 279–287.

Muñoz P, Munné-Bosch S. 2018. Photo-oxidative stress during leaf, flower and fruit development. *Plant Physiology* 176: 1004–1014.

Nagel R, Bernholz C, Vranová E, Košuth J, Bergau N, Ludwig S, Wessjohann L, Gershenzon J, Tissier A, Schmidt A. 2015. *Arabidopsis thaliana* isoprenyl diphosphate synthases produce the C 25 intermediate, geranylfarnesyl diphosphate. *The Plant Journal* 84: 847–859.

Nisar N, Li L, Lu S, Khin NC, Pogson BJ. 2015. Carotenoid metabolism in plants. *Molecular Plant* 8: 68–82.

Obata T, Fernie AR. 2012. The use of metabolomics to dissect plant responses to abiotic stresses. *Cellular and Molecular Life Sciences* 69: 3225–3243.

Okada K, Saito T, Nakagawa T, Kawamukai M, Kamiya Y. 2000. Five geranylgeranyl diphosphate synthases expressed in different organs are localized into three subcellular compartments in Arabidopsis. *Plant Physiology* 122: 1045–1056.

Orlova I, Nagegowda DA, Kish CM, Gutensohn M, Maeda H, Varbanova M, Fridman E, Yamaguchi S, Hanada A, Kamiya Y *et al.* 2009. The small subunit of snapdragon geranyl diphosphate synthase modifies the chain length specificity of tobacco geranylgeranyl diphosphate synthase *in planta*. *Plant Cell* 21: 4002–4017.

Pulido P, Perello C, Rodríguez-Concepción M. 2012. New insights into plant isoprenoid metabolism. *Molecular Plant* 5: 964–967.

Pulido P, Toledo-Ortiz G, Phillips MA, Wright LP, Rodríguez-Concepción M. 2013. Arabidopsis J-protein J20 delivers the first enzyme of the plastidial isoprenoid pathway to protein quality control. *Plant Cell* 25: 4183–4194.

Rodriguez-Concepcion M, Avalos J, Bonet ML, Boronat A, Gomez-Gomez L, Hornero-Mendez D, Limon MC, Meléndez-Martínez AJ, Olmedilla-Alonso B, Palou A *et al.* 2018. A global perspective on carotenoids: metabolism, biotechnology, and benefits for nutrition and health. *Progress in Lipid Research* 70: 62–93.

Rodríguez-Concepción M, Boronat A. 2015. Breaking new ground in the regulation of the early steps of plant isoprenoid biosynthesis. *Current Opinion in Plant Biology* 25: 17–22.

Ruiz-Lozano JM, Aroca R, Zamarreño ÁM, Molina S, Andreo-Jiménez B, Porcel R, García-Mina JM, Ruyter-Spira C, López-Ráez JA. 2016. Arbuscular mycorrhizal symbiosis induces strigolactone biosynthesis under drought and improves drought tolerance in lettuce and tomato. *Plant, Cell & Environment* 39: 441–452.

Ruiz-Sola MÁ, Barja MV, Manzano D, Llorente B, Schipper B, Beekwilder J, Rodriguez-Concepcion M. 2016a. A single arabidopsis gene encodes two differentially targeted geranylgeranyl diphosphate synthase isoforms. *Plant Physiology* 172: 1393–1402.

Ruiz-Sola MÁ, Coman D, Beck G, Barja MV, Colinas M, Graf A, Welsch R, Rütimann P, Bühlmann P, Bigler L *et al.* 2016b. Arabidopsis GERANYLGERANYL DIPHOSPHATE SYNTHASE 11 is a hub isozyme required for the production of most photosynthesis-related isoprenoids. *New Phytologist* 209: 252–264.

Ruiz-Sola MÁ, Rodríguez-Concepción M. 2012. Carotenoid biosynthesis in Arabidopsis: a colorful pathway. *The Arabidopsis book* 10: e0158.

Sandmann G. 2015. Carotenoids of biotechnological importance. *Advances in Biochemical Engineering/Biotechnology* 148: 449–467.

Schiml S, Fauser F, Puchta H. 2016. CRISPR/Cas-mediated site-specific mutagenesis in *Arabidopsis thaliana* using Cas9 nucleases and paired nickases. *Methods in Molecular Biology* 1469: 111–122.

Simon P. 2003. Q-Gene: processing quantitative real-time RT-PCR data. *Bioinformatics* 19: 1439–1440.

Sparkes IA, Runions J, Kearns A, Hawes C. 2006. Rapid, transient expression of fluorescent fusion proteins in tobacco plants and generation of stably transformed plants. *Nature Protocols* 1: 2019–2025.

Stauder R, Welsch R, Camagna M, Kohlen W, Balcke GU, Tissier A, Walter MH. 2018. Strigolactone levels in dicot roots are determined by an ancestral symbiosis-regulated clade of the PHYTOENE SYNTHASE gene family. *Frontiers in Plant Science* 9: 255.

Sun T, Yuan H, Cao H, Yazdani M, Tadmor Y, Li L. 2018. Carotenoid metabolism in plants: the role of plastids. *Molecular Plant* 11: 58–74.

Tholl D. 2015. Biosynthesis and biological functions of terpenoids in plants. *Advances in Biochemical Engineering/Biotechnology* 148: 63–106.

Vranová E, Coman D, Gruissem W. 2013. Network analysis of the MVA and MEP pathways for isoprenoid synthesis. *Annual Review of Plant Biology* 64: 665–700.

Walter MH, Stauder R, Tissier A. 2015. Evolution of root-specific carotenoid precursor pathways for apocarotenoid signal biogenesis. *Plant Science* 233: 1–10.

Wang C, Chen Q, Fan D, Li J, Wang G, Zhang P. 2016. Structural analyses of short-chain prenyltransferases identify an evolutionarily conserved GFPPS Clade in Brassicaceae plants. *Molecular Plant* 9: 195–204.

Wang G, Dixon RA. 2009. Heterodimeric geranyl(geranyl)diphosphate synthase from hop (*Humulus lupulus*) and the evolution of monoterpene biosynthesis. *Proceedings of the National Academy of Sciences, USA* 106: 9914–9919.

Wang J, Lin H-X, Su P, Chen T, Guo J, Gao W, Huang L-Q. 2019. Molecular cloning and functional characterization of multiple geranylgeranyl pyrophosphate synthases (ApGGPPS) from *Andrographis paniculata*. *Plant Cell Reports* 38: 117–128.

Wang Q, Huang X-Q, Cao T-J, Zhuang Z, Wang R, Lu S. 2018. Heteromeric geranylgeranyl diphosphate synthase contributes to carotenoid biosynthesis in ripening fruits of red pepper (*Capsicum annuum* var. *conoides*). *Journal of Agriculture and Food Chemistry* 66: 11691–11700.

Yuan H, Zhang J, Nageswaran D, Li L. 2015. Carotenoid metabolism and regulation in horticultural crops. *Horticulture Research* 2: 15036.

Zhang M, Su P, Zhou Y-J, Wang X-J, Zhao Y-J, Liu Y-J, Tong Y-R, Hu T-Y, Huang L-Q, Gao W. 2015. Identification of geranylgeranyl diphosphate synthase genes from *Tripterygium wilfordii*. *Plant Cell Reports* 34: 2179–2188.

Zhang M, Yuan B, Leng P. 2009. The role of ABA in triggering ethylene biosynthesis and ripening of tomato fruit. *Journal of Experimental Botany* 60: 1579–1588.

Zhou F, Pichersky E. 2020. The complete functional characterisation of the terpene synthase family in tomato. *New Phytologist* 226: 1341–1360.

Zhou F, Wang C-Y, Gutensohn M, Jiang L, Zhang P, Zhang D, Dudareva N, Lu S. 2017. A recruiting protein of geranylgeranyl diphosphate synthase controls metabolic flux toward chlorophyll biosynthesis in rice. *Proceedings of the National Academy of Sciences, USA* 114: 6866–6871.

Zhu XF, Suzuki K, Okada K, Tanaka K, Nakagawa T, Kawamukai M, Matsuda K. 1997a. Cloning and functional expression of a novel geranylgeranyl pyrophosphate synthase gene from *Arabidopsis thaliana* in *Escherichia coli*. *Plant and Cell Physiology* 38: 357–361.

Zhu XF, Suzuki K, Saito T, Okada K, Tanaka K, Nakagawa T, Matsuda H, Kawamukai M. 1997b. Geranylgeranyl pyrophosphate synthase encoded by the newly isolated gene GGPS6 from *Arabidopsis thaliana* is localized in mitochondria. *Plant Molecular Biology* 35: 331–341.

Zouine M, Maza E, Djari A, Lauvernier M, Frasse P, Smouni A, Pirrello J, Bouzayen M. 2017. TomExpress, a unified tomato RNA-Seq platform for visualization of expression data, clustering and correlation networks. *The Plant Journal* 92: 727–735.

Supporting Information

Additional Supporting Information may be found online in the Supporting Information section at the end of the article.

Fig. S1 Subcellular localisation of tomato GGPPS proteins.

Fig. S2 Purification of recombinant GGPPS proteins for *in vitro* activity assays.

Fig. S3 Biochemical activity of purified recombinant GGPPS proteins.

Fig. S4 Transcript levels of tomato genes in different tissues.

Fig. S5 Gene co-expression network (GCN) analysis of tomato plastidial *GGPPS* genes in leaf and fruit tissues.

Fig. S6 DNA sequence alignment of *SlG2* CRISPR mutants.

Fig. S7 DNA sequence alignment of *SlG3* CRISPR mutants.

Fig. S8 Protein alignments of WT and mutant SlG2 and SlG3 sequences.

Fig. S9 Fruit ripening initiation and progression in WT and mutant plants.

Fig. S10 Relative levels of plastidial isoprenoids in mature green fruits from WT and mutant lines.

Fig. S11 PCR-based genotyping of nongerminating F2 seeds from the cross of *slg2-2* and *slg3-1* mutant plants.

Methods S1 Growth conditions, sample collection and phenotypic analyses.

Methods S2 Constructs.

Methods S3 RNA isolation and cDNA synthesis.

Methods S4 GGPPS activity determination.

Methods S5 Subcellular localisation assays.

Methods S6 Co-immunoprecipitation assays.

Methods S7 Isoprenoid analysis.

Table S1 Primers used in this work.

Table S2 Constructs and cloning details.

Table S3 List of tomato GGPPS-like sequences.

Table S4 List of plastidial isoprenoid-related genes used for the tomato GGPPS GCN analyses.

Table S5 List of expression datasets in the TomExpress database used for the generation of the tomato GGPPS GCN in leaf and fruit tissues.

Table S6 Co-expression of tomato GGPPS paralogues (guide genes) with isoprenoid-related genes (query genes) in leaf and fruit tissues.

Table S7 Levels of GGPP-derived metabolites detected by HPLC.

Table S8 Relative levels of metabolites detected by GC-MS in samples from WT and mutant young leaves.

Table S9 Parameters used for peak annotation in leaves.

Table S10 Relative levels of metabolites detected by GC-MS in samples from WT and mutant B + 10 fruit.

Table S11 Parameters used for peak annotation in B + 10 fruit.

Please note: Wiley Blackwell are not responsible for the content or functionality of any Supporting Information supplied by the authors. Any queries (other than missing material) should be directed to the *New Phytologist* Central Office.

SUPPORTING INFORMATION

Several geranylgeranyl diphosphate synthase isoforms supply metabolic substrates for carotenoid biosynthesis in tomato

M. Victoria BARJA, Miguel EZQUERRO, Stefano BERETTA, Gianfranco DIRETTO, Igor FLOREZ-SARASA, Elisenda FEIXES, Alessia FIORE, Rumyana KARLOVA, Alisdair R. FERNIE, Jules BEEKWILDER, Manuel RODRIGUEZ-CONCEPCION

METHODS

Method S1. Growth conditions, sample collection and phenotypic analyses.
Tomato (*Solanum lycopersicum* var. MicroTom) seeds were surface-sterilized by a 15 min incubation in 25 mL of 40% bleach containing a drop of Tween-20 followed by 3 consecutive 10 min washes with sterilized milli-Q water. Sterile seeds were germinated on plates with solid 0.5x Murashige and Skoog medium without vitamins or sucrose. The medium was supplemented with kanamycin (100 µg/mL) when required to select transgenic plants. After stratification at 4 °C in the dark for at least 3 days, plates were incubated in a climate-controlled growth chamber at 24 °C with a photoperiod of 10 h of darkness for 14 h of fluorescent white light at a photosynthetic photon flux density of 140 µmol m^{-2} s^{-1}. After 1 to 2 weeks, seedlings were transferred to soil and grown under standard greenhouse conditions (14 h light at 27 ± 1 °C and 10 h dark at 22 ± 1 °C). Photosynthetic activity was assessed by measuring chlorophyll *a* fluorescence with a MAXI-PAM fluorometer (Walz). The effective quantum yield φPSII (ΔF/Fm') of young and mature tomato leaves was measured as (Fm'−Fs)/Fm', where Fm' and Fs are the maximum and the minimum fluorescence of light exposed plants, respectively. The light intensity chosen was 21 PAR (actinic light, AL=2). The results are presented as the average of three biological replicates and four different leaf areas for each replicate. For the analysis of flowering time, at least five independent plants of each genotype were used. Flowering time was assessed by counting the number of days from germination until the first flower was fully opened (anthesis) or the number of leaves in the plant at this first anthesis day. Fruit pigmentation was measured using the TomatoAnalyzer 4.0 software (https://vanderknaaplab.uga.edu/tomato_analyzer.html). Average Red Color of three different whole tomatoes was quantified using the default red color calibrator sorted by the software as standard. For deetiolation experiments, seeds were sown on sterile water-soaked cotton in plastic containers. After stratification, seeds were exposed to fluorescent white light for 2-4 hours at 22°C to induce germination. The containers were then covered with a double layer of aluminum foil and kept in darkness at 22 °C. After one week, seedlings were exposed to light and samples were harvested after 0, 6 and 24 h. Control samples were germinated and grown under continuous light and collected at the 0 h time point. Leaf samples were collected from four-week-old plants. Young leaf samples correspond to growing leaflets from the fifth and sixth true leaves, and mature leaf samples correspond to fully expanded leaflets from the third or fourth leaf. Tomato fruit pericarp samples were collected at four ripening stages based on days post-anthesis (DPA) or days post-breaker (DPB): mature green (~30 DPA), breaker (~35 DPA), orange (~38-40 DPA) and red (~45-50 DPA or 10 DPB). Full seedlings, leaflets, and pericarp samples were frozen in liquid nitrogen immediately after collection, freeze-dried and stored at -80 °C.

Method S2. Constructs. Full-length cDNAs encoding SlG1-5 and PSY1-2 proteins without their stop codons were amplified by PCR and cloned via BP clonase into pDONR207 entry plasmid using Gateway (GW) technology (Invitrogen). Full-length sequences were then subcloned through an LR reaction into pGWB405 plasmid for subcellular localization assays, or into pGWB414 and pGWB420 plasmids for co-immunoprecipitation experiments. Constructs in pGWB405, pGWB414 and pGWB420 vectors harbor GFP, 3x-HA and 10x-Myc tags, respectively. These tag sequences are fused to the C-terminus of each cloned element and the expression module is controlled by the CaMV 35S promoter. For recombinant protein production in *E. coli*, SlG1-3 versions lacking the predicted transit peptide for plastid import were amplified from pGWB405 constructs, cloned into pDONR207 plasmid, and then subcloned into pET32-GW plasmid (fusing a 6x-His tag at the N-terminal end of the cloned fragments) under the control of the T7 promoter. For CRISPR-Cas9-mediated disruption of *SlG2* and *SlG3*, two single guide RNAs (sgRNA) sequences were designed encompassing an *EcoRI* and a *PstI* restriction site for *SlG2* and *SlG3* genes, respectively (Figures S6 and S7). A pair of primers for each guide was designed, denaturalized and assembled into pENC1.1 (pENTRY) vector previously digested with *BbsI.* The entry vectors contained the corresponding sgRNA expression cassette flanked by *Bsu36I* and *MluI* restriction sites, and by GW recombinant sites to allow both types of interchange with a pDE-Cas9 plasmid providing kanamycin resistance (pDESTINY). The final binary vectors were generated in a two-step cloning process that involved *Bsu36I* and *MluI* digestion-ligation of the first sgRNA into the pDE-Cas9 vector followed by an LR reaction to subclone the second sgRNA of each gene into the pDE-Cas9 vector already containing the first sgRNA. For activity assays in *E. coli*, full-length *SlG2*, *SlG3*, *slg2-1*, *slg2-2*, *slg3-1* and *slg3-2* sequences were amplified from genomic DNA of the corresponding lines and cloned into the *SmaI* site of the pBluescript SK+ plasmid. All constructs were confirmed by restriction mapping and DNA sequencing. Information about primers used and cloning details are described in Tables S1 and S2, respectively.

Method S3. RNA isolation and cDNA synthesis. Total RNA was isolated from tomato freeze-dried tissue (seedlings, leaves or fruit pericarp) using the Maxwell® RSC Plant RNA Kit with the Maxwell® RSC Instruments (Promega) following the manufacturer's instructions. RNA was quantified using a NanoDropTM 8000 spectrophotometer (ThermoFischer Scientific) and checked for integrity by agarose gel electrophoresis. The Transcriptor First Strand cDNA Synthesis Kit (Roche) was used to reverse transcribe 0.5 µg of extracted RNA into 20 µL of cDNA, which was subsequently diluted ten-fold and stored at -20 °C for further analysis. Relative mRNA abundance was evaluated via Real-Time Quantitative Polymerase Chain Reaction (RT-qPCR) in a reaction volume of 20 µL containing 10 µL of the LightCycler 480 SYBR Green I Master Mix (Roche), 0.3 µM of each specific forward and reverse primer (Table S1) and 5 µL of cDNA. The RT-qPCR was carried out on a LightCycler 480 Real-Time PCR System (Roche). Three independent biological replicates of each condition and at least two technical replicates of each biological replicate were performed. Primer efficiencies were calculated using serial dilutions of genomic or plasmidic DNA.

Method S4. GGPPS activity determination. Constructs to produce different truncated GGPPS protein versions were generated in the pET32-GW vector (Table S2). Competent *E. coli Rosetta 2* (DE3) cells (Novagen) were separately transformed with each construct and single transformants were grown overnight at 37 °C in 5 mL of LB medium supplemented with appropriate antibiotics. Then, 250 µL of each overnight culture were diluted in 25 mL 2xYT medium with the required antibiotics and incubated at 37 °C and 250 rpm until reaching an OD600 between 0.5 and 0.8. After inducing the production of the recombinant proteins with 1 mM IPTG, the cultures were grown overnight at 18 °C and 250 rpm. Bacterial cells were harvested by centrifugation at 2,000 *g* for 15 min and pellets were resuspended in 1 mL *Assay* buffer (15 mM MOPSO, 12.5% v/v glycerol, 1 mM ascorbic acid, pH 7.0, 1 mM $MgCl_2$, 2 mM DTT). About 0.2 g of

2

zirconium/silica beads 0.1 mm (BioSpec Products) were added and bacterial lysis was carried out in two rounds of shaking for 10 s at a speed of 6.5 in a FastPrep machine (FP120 Bio101 Savant). Cell lysates were subsequently centrifuged for 10 min at 13,000 g and 4 °C, and supernatants were collected for SDS-PAGE and GGPP activity assays. Enzymatic assays were performed in Eppendorf tubes in a final volume of 200 µL containing 25 µL of cell extract, 150 µM IPP and 50 µM DMAPP in *Assay* buffer supplemented with 5 mM Na_3O_4V. The reaction mix was incubated for 2 h at 30 °C in mild agitation and stopped by adding 800 µL of 100% methanol / 0.5% formic acid. After vortexing, samples were sonicated for 15 min and centrifuged at maximum speed for 10 min. Supernatants were then evaporated in a SpeedVac concentrator and 80 µL of 100% methanol / 0.65% formic acid were added to the remnant sample. After centrifugation at maximum speed for 15 min, the supernatants were transferred to glass vials. The detection of prenyl diphosphate products by Liquid Chromatography-Mass Spectrometry (LC-MS) using Xcalibur™ software (ThermoFischer Scientific) for data acquisition and visualization. Kinetic parameters were calculated using 3 µg of purified SlG1, SlG2, SlG3 and AtG11 enzymes. pET32 constructs were used to produce 6xHis-tagged recombinant enzymes (Table S2) and protein purification from *E. coli Rosetta* cells was carried out using nickel-nitrilotriacetic acid (Ni-NTA) agarose (Qiagen) (Barja and Rodríguez-Concepción, 2020). IPP and DMAPP substrates and FPP and GGPP standards were obtained from Echelon Biosciences.

Method S5. Subcellular localization assays. *A. tumefaciens* GV3101 cells were transformed with pGWB405-based constructs (Table S2) and grown on LB plates at 28 °C for 3 days. A single PCR-confirmed colony per construct was grown overnight at 28 °C in 5 mL antibiotic-supplemented LB media and 500 µL of the grown culture were then inoculated in 20 mL of fresh medium. After another overnight incubation, bacterial cells were pelleted and resuspended in infiltration buffer (10 mM MES pH5.5-6, 10 mM $MgSO_4$, 150 µM acetosyringone) to a final OD600 of 0.5. To prevent silencing, *N. benthamiana* leaves were co-infiltrated with a second *Agrobacterium* strain harboring a HC-Pro silencing suppressor. A 1:1 mixture of the two cultures was infiltrated with a syringe in the abaxial part of leaves from 4 to 6-week old *N. benthamiana* plants. GFP signal and chlorophyll autofluorescence were detected with an Olympus FV 1000 confocal laser-scanning microscope using an argon laser for excitation (at 488 nm) and a 500–510 nm filter (for GFP) or a 610–700 nm filter (for chlorophyll). All images were acquired using the same confocal parameters.

Method S6. Co-immunoprecipitation assays. Constructs encoding Myc- and HA-tagged tomato GGPPS and PSY proteins (Table S2) were transformed into *A. tumefaciens* GV3101 strains. A plasmid containing the Arabidopsis phosphoribulokinase protein with a Myc tag (pGWB417_PRK-Myc) was kindly provided by Dr. Ernesto Llamas and used as a negative control. Different *Agrobacterium* infiltration mixtures were prepared and infiltrated into *N. benthamiana* leaves, and 3 days later 1.2 g of agroinfiltrated leaf tissue was frozen in liquid nitrogen and directly stored at -80 ºC until use. For crude extracts preparation, frozen leaf samples were ground in liquid nitrogen and incubated in 4 ml lysis buffer (50 mM Tris-HCl pH7.5, 150 mM NaCl, 5% glycerol, 0.05% NP-40, 1 mM $MgCl_2$, 0.5 mM PMSF, 1X Sigma protease inhibitor, 10 mM DTT, 2% PVPP) at 4 ºC for 15 min using a rotator to form a homogeneous suspension, that was then pre-clarified at 3,000 g for 15 min. Supernatants were cleaned by centrifugation at 16,000 g for 30 min and used for protein quantification. Crude extracts were then adjusted to the same volume and protein concentration with lysis buffer lacking PVPP. An aliquot of each adjusted crude extract was boiled for 10 min in SDS-loading buffer and stored at -20 ºC as input sample. 500 µL of each crude extract were incubated overnight with 1 µL of monoclonal αMyc antibody (Sigma) in a rotator at 4 ºC. Immunoprecipitation of αMyc interacting protein/complexes was carried out using Pierce Protein A/G Magnetic Beads (ThermoFischer Scientific). After pre-washing the magnetic beads (50 mM Tris-HCl pH7.5, 500 mM NaCl, 5% glycerol, 0.05% NP-40, 1 mM $MgCl_2$,

0.5 mM PMSF, 1X Sigma protease inhibitor, 10 mM DTT), the Co-IP sample (crude extract + αMyc antibody) was added and incubated with the beads at room temperature for 1 h with shaking. The beads were then collected with a magnetic stand and repeatedly washed with washing buffer and water. After removing the water from the last washing step, 100 μL of SDS-PAGE loading buffer were added to the beads and boiled for 10 min. Afterwards, the beads were magnetically removed from the supernatants containing the immunoprecipitated complexes and stored at -20 ºC. The presence of Myc- and HA-tagged proteins in input and Co-IP samples were detected by immunoblot analyses using 1:5000-diluted αMyc (Sigma) and 1:1000-diluted αHA (Roche) as primary antibodies. Horseradish peroxidase (HRP)-conjugated secondary antibodies against mouse and rat IgGs were used in a 1:10000 dilution. WesternBright ECL Western blotting detection kit (Advansta) and Amersham ECL Prime Western Blotting Detection Kit (GE Healthcare) were used for detection and the signal was visualized using the ChemiDoc Touch Imaging System (Bio-Rad).

Method S7. Isoprenoid analysis. Carotenoids, chlorophylls and tocopherols were extracted as follows. A mix was prepared in 2 mL Epperdorf tubes with ca. 4 mg of freeze-dried leaf tissue, 375 μL of methanol as extraction solvent and 25 μL of a 10 % (w/v) solution of canthaxanthin (Sigma) in chloroform as internal control. After vortexing the samples for 10 s and lysing the tissue with 4 mm glass beads for 1 min at 30 Hz in the TissueLyser II (Qiagen), 400 μL of Tris-HCl pH:7.5 were added and the samples were again mixed for 1 min in the TissueLyser. Next, 800 μL of chloroform were added and the mixture was again shaken for 1 min in the TissueLyser. Samples were then centrifuged for 5 min at maximum speed at 4 ºC. The lower organic phase was placed in a new 1.5 mL tube and evaporated using a SpeedVac. Fruit isoprenoids were extracted using 15 mg of freeze-dried tissue and 1 ml of hexane/acetone/methanol 2:1:1 as extraction solvent. After vortexing and lysing the tissue with the TissueLyser as described for leaves, 100 μL of milli-Q water were added. Then, 1 min of TissueLyser was carried out again and samples were centrifuged for 3 min at 500 g and 4 ºC. The organic phase was transferred to a 1.5 mL tube and the rest was re-extracted by adding 1 mL of hexane/acetone/methanol 2:1:1 solvent, TissueLyser-mixing for 1 min and centrifuging for 5 min at maximum speed and 4 ºC. The new organic phase was mixed with that previously extracted and evaporated using the SpeedVac system. Extracted metabolites from leaf and fruit pericarp samples were resuspended in 200 μL of acetone by using an ultrasound bath (Labolan) and filtered with 0.2 μm filters into amber-colored 2 mL glass vials. Separation and detection was next performed using an Agilent 1200 series HPLC system (Agilent Technologies). Eluting chlorophylls and carotenoids were monitored using a photodiode array detector whereas tocopherols were identified using a fluorescence detector. Peak areas of chlorophylls (650 nm), carotenoids (470 nm for lycopene, lutein, β-carotene, violaxanthin, neoxanthin and canthaxanthin or 280 nm for phytoene), and tocopherols (330 nm) were determined using the Agilent ChemStation software. Quantification was performed by comparison with commercial standards (Sigma).

FIGURES
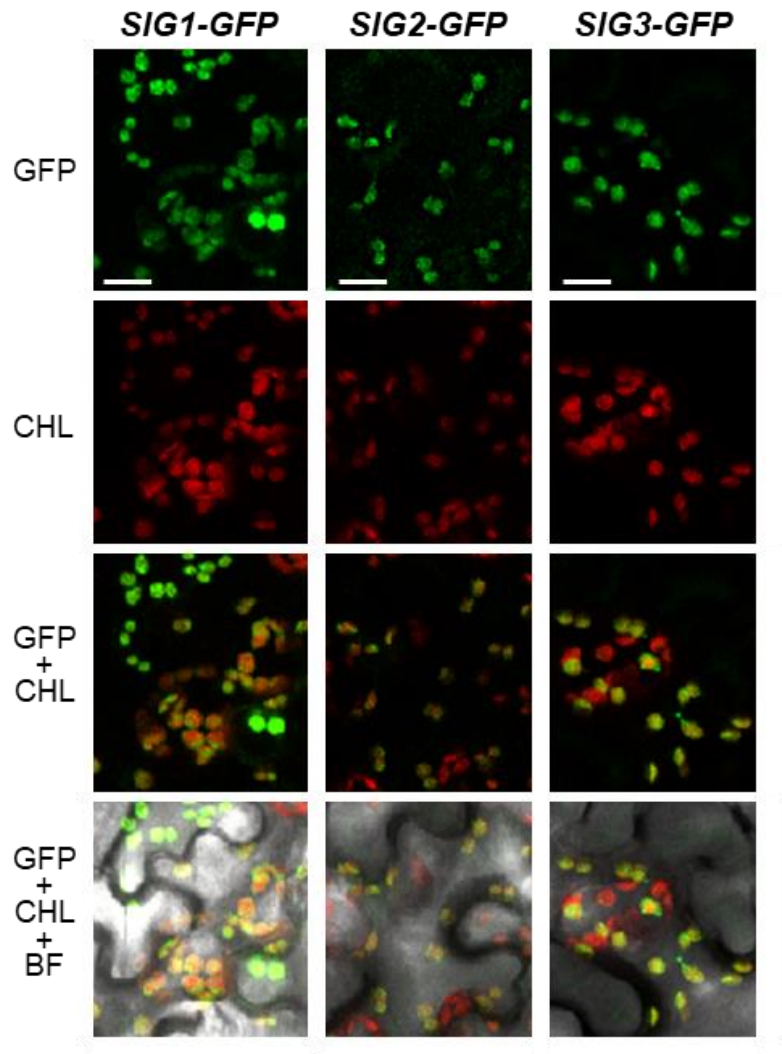
Figure S1. Subcellular localization of tomato GGPPS proteins. Representative confocal microscopy images of *N. benthamiana* leaf cells transiently expressing the indicated GFP fusion proteins are shown. For each construct, GFP fluorescence (GFP), chlorophyll autofluorescence (CHL) and merged images of them either alone (GFP+CHL) or overlapped with the bright field image (GFP+CHL+BF) are shown for the same field. Bars, 10 μm.
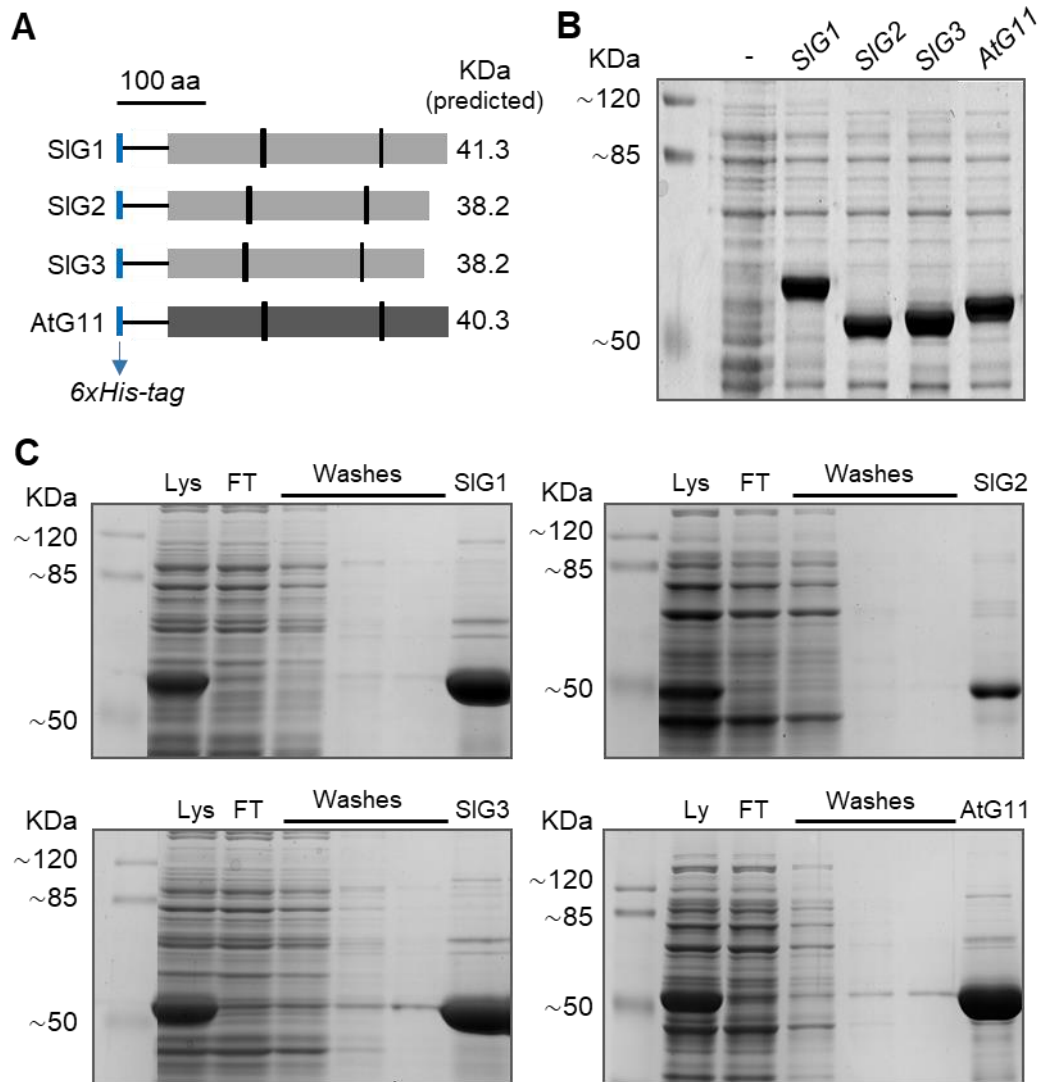
Figure S2. Purification of recombinant GGPPS proteins for *in vitro* activity assays.
(A) Schematic representation of the purified GGPPS enzyme versions lacking the predicted plastid-targeting peptide and fused to a 6xHis-tag (blue) in the N-terminal end.
(B) Coomassie-Blue stained SDS-PAGE of total protein extracts from *E. coli Rosetta* cells transformed with constructs to express the indicated GGPPS versions or an empty plasmid (marked as "-"). After IPTG induction, a 10 µL aliquot of each culture was boiled for 10 min in SDS-loading buffer and run in a gel. A protein size ladder is shown in the left. **(C)** Coomassie-Blue stained gels showing the purification steps of the indicated proteins. The enzymes were purified from soluble lysates (Lys) of *E. coli* cells overproducing the corresponding recombinant protein. Lysates were separately incubated with Ni-NTA beads and the staining of the flow-through (FT) shows that most of the recombinant protein was retained in the Ni-NTA column. After several washes with 20 mM imidazole to remove non-specific proteins attached to the column, His-tagged enzymes were eluted using 150 mM imidazole. Purified proteins were then desalted, quantified and stored with glycerol 40% in the freezer until use for activity assays.
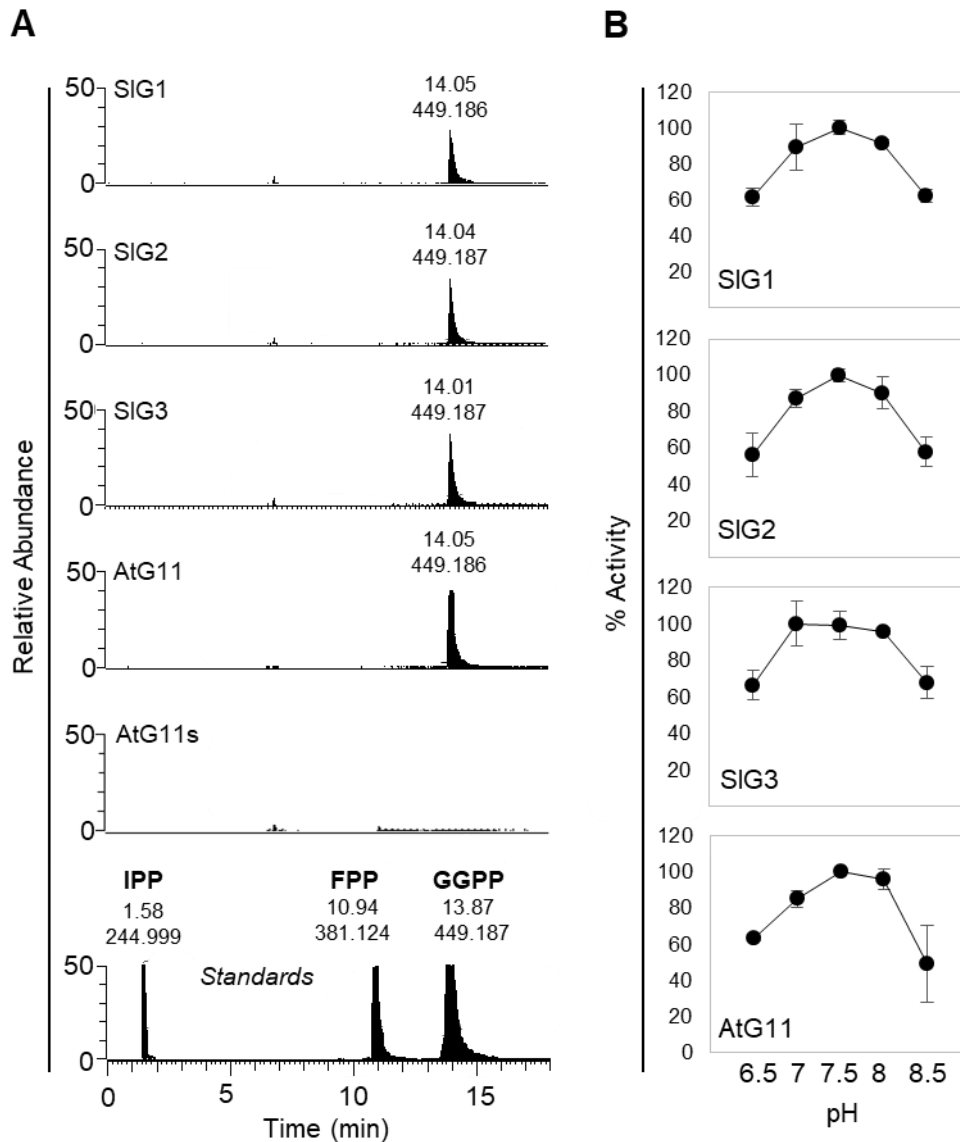
Figure S3. Biochemical activity of purified recombinant GGPPS proteins. (A) LC-MS chromatograms of reaction products. Extracts of *E. coli* cells overproducing the indicated recombinant proteins (with an N-terminal 6x-His tag instead of their predicted plastid-targeting peptide) were incubated with IPP and DMAPP. Prenyl diphosphate products in the *in vitro* assays were detected by LC-MS using mass-to-charge (m/z) ratios of 313.061 (GPP), 381.123 (FPP), 449.186 (GGPP) and 518.254 (GFPP). Retention times and m/z values of available standards is also shown in the bottom plot. **(B)** Optimal pH determination for the activity of each GGPPS assayed. Purified recombinant proteins were incubated with IPP and DMAPP under different pH conditions. Activity values are represented as the percentage of activity relative to the maximum activity obtained. Data correspond to the mean ± SD of n=3 independent replicates.
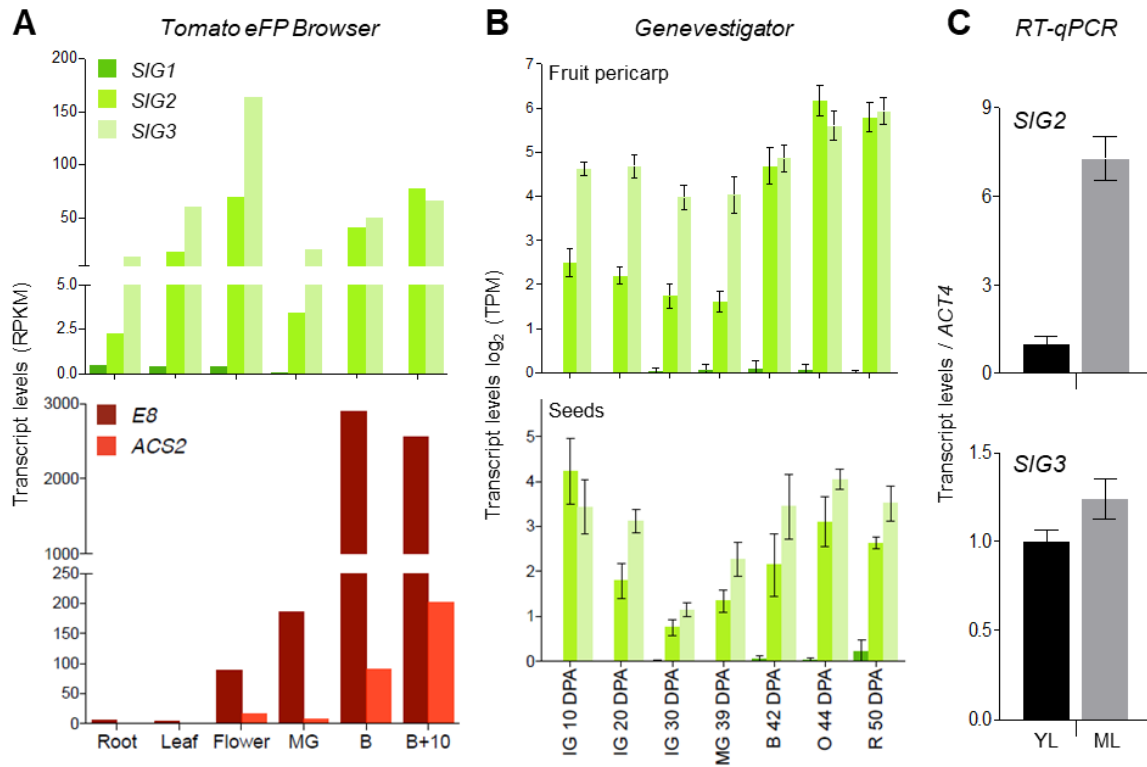
Figure S4. Transcript levels of tomato genes in different tissues. Abbreviations: DPA, days post-anthesis; IG, immature green; MG, mature green; B, breaker; O, orange, R, red; YL, young leaves; ML, mature leaves. **(A)** RNAseq data retrieved from the *Tomato eFP Browser* database (http://bar.utoronto.ca/efp_tomato/cgi-bin/efpWeb.cgi). Plots show the transcript levels of *SIG1-3, E8 (Solyc09g089580)* and *ACS2 (Solyc01g095080)* genes in root, leaf, flower and fruit pericarp during ripening. Expression data are represented as RPKM (Reads per Kilobase of transcript per Million mapped reads). **(B)** RNAseq data obtained from GeneInvestigator (https://genevestigator.com/). Plots show the transcript levels of *SIG1-3* genes in fruit pericarp and seeds during development. Levels are represented as $\log_2$ TPM (Transcripts per Million mapped reads). **(C)** RT-qPCR analysis of *SIG2* and *SIG3* transcript levels in young and mature leaves from WT plants. Expression values were normalized using *ACT4* and and they are shown relative to YL samples. Data correspond to the mean±SD of n=3 independent biological replicates.
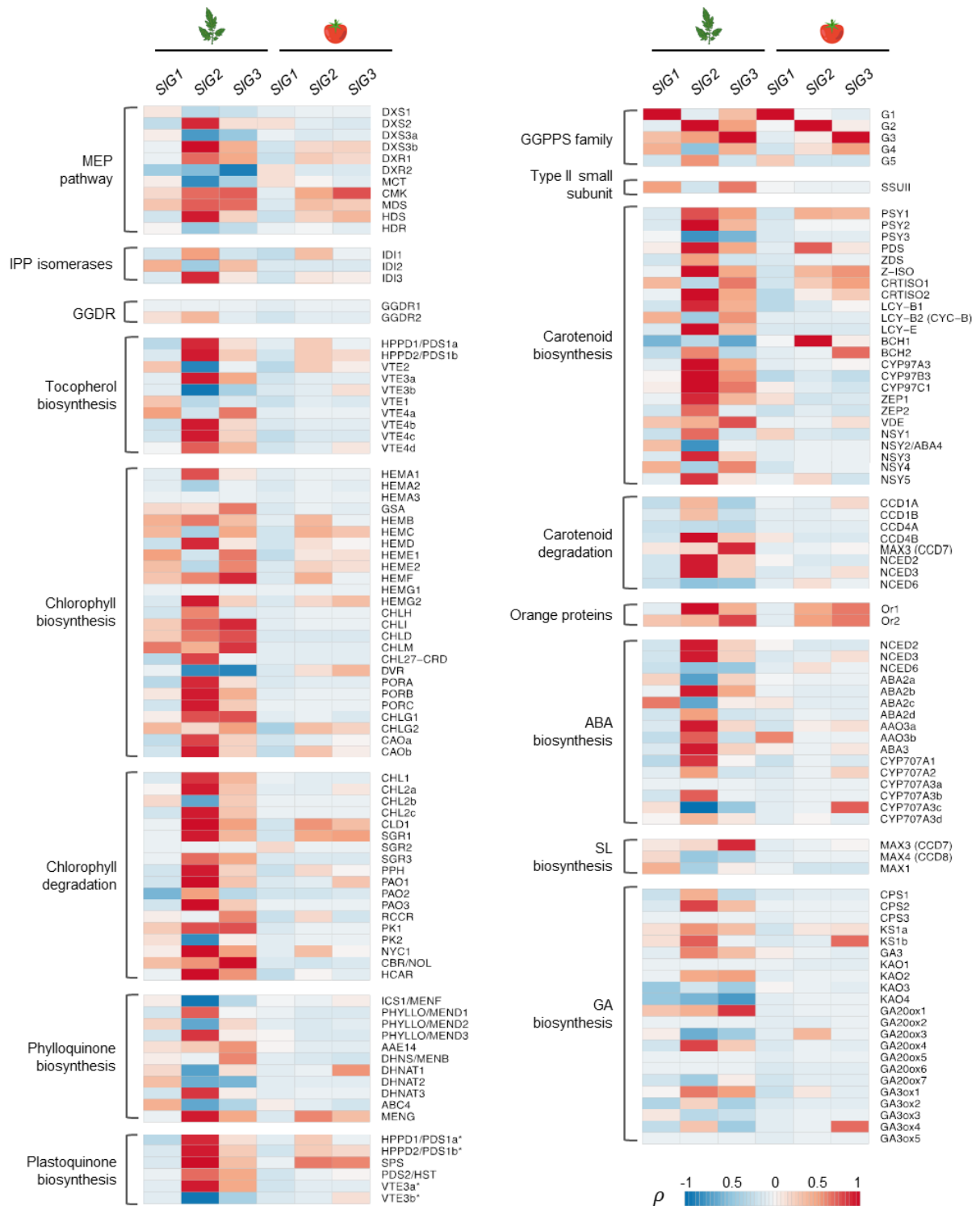
Figure S5. Gene co-expression network (GCN) analysis of tomato plastidial *GGPPS* genes in leaf and fruit tissues. Pairwise Pearson correlations (ρ) between the expression of genes encoding GGPPS isoforms and enzymes from the indicated plastidial isoprenoid pathways upstream and downstream of GGPP are represented as a heatmap. Gene abbreviations and accessions are listed in Table S4, leaf and fruit datasets used for the analysis are indicated in Table S5, and positive co-relation ρ values are shown in Table S6.

```
SlG2    ATGAGATCTATGAACCTTGTTGATTCATGGGGTCAAGCTTGTTTAGTTATCAATCAATCTTTACCTTACAATTCGTTTAA    80
slg2-1  ATGAGATCTATGAACCTTGTTGATTCATGGGGTCAAGCTTGTTTAGTTATCAATCAATCTTTACCTTACAATTCGTTTAA    80
slg2-2  ATGAGATCTATGAACCTTGTTGATTCATGGGGTCAAGCTTGTTTAGTTATCAATCAATCTTTACCTTACAATTCGTTTAA    80
        ********************************************************************************

SlG2    TGGATTGATGAAAATCAATTCGAAAAATCGAAAAATTTTGAAACAGAGTTTATCTTATAGAACATTTTCATCTGTAACTG    160
slg2-1  TGGATTGATGAAAATCAATTCGAAAAATCGAAAAATTTTGAAACAGAGTTTATCTTATAGAACATTTTCATCTGTAACTG    160
slg2-2  TGGATTGATGAAAATCAATTCGAAAAATCGAAAAATTTTGAAACAGAGTTTATCTTATAGAACATTTTCATCTGTAACTG    160
        ********************************************************************************

SlG2    TTTCAGCTATTGCTACCAATGAGAAAGTTGTTATGGAAAAAGAAGAATTTAATTTCAAGGTTTACGTAGCTGAAAAGGCG    240
slg2-1  TTTCAGCTATTGCTACCAATGAGAAAGTTGTTATGGAAAAAGAAGAATTTAATTTCAAGGTTTACGTAGCTGAAAAGGCG    240
slg2-2  TTTCAGCTATTGCTACCAATGAGAAAGTTGTTATGGAAAAAGAAGAATTTAATTTCAAGGTTTACGTAGCTGAAAAGGCG    240
        ********************************************************************************

SlG2    ATTTGTGTAAATAAAGCTTTGGATGAGGCTATAATGGTAAAAGACCCACCTAAGATCCATGAAGCAATGCGTTATTCGCT    320
slg2-1  ATTTGTGTAAATAAAGCTTTGGATGAGGCTATAATGGTAAAAGACCCACCTAAGATCCATGAAGCAATGCGTTATTCGCT    320
slg2-2  ATTTGTGTAAATAAAGCTTTGGATGAGGCTATAATGGTAAAAGACCCACCTAAGATCCATGAAGCAATGCGTTATTCGCT    320
        ********************************************************************************

SlG2    TCTCGCCGGCGGGAAGAGAGTCCGGCCGATGCTCTGTCTTGCTGCCTGTGAACTTGTTGGGGGGAAACCAAGGGAATGCTA    400
slg2-1  TCTCGCCGGCGGGAAGAGAGTCCGGCCGATGCTCTGTCTTGCTGCCTGTGAACTTGTTGGGGGGAAACCAAGGGAATGCTA    400
slg2-2  TCTCGCCGGCGGGAAGAGAGTCCGGCCGATGCTCTGTCTTGCTGCCTGTGAACTTGTTGGGGGGAAACCAAGGGAATGCTA    400
        ********************************************************************************

                                                              SIG2 CRISPR Geno F
SlG2    TGGCGGCTGCTTGTGCTGTTGAGATGATACATACTATGTCTCTAATTCATGATGATTTGCCTTGTATGGATGACGACGAT    480
slg2-1  TGGCGGCTGCTTGTGCTGTTGAGATGATACATACTATGTCTCTAATTCATGATGATTTGCCTTGTATGGATGACGACGAT    480
slg2-2  TGGCGGCTGCTTGTGCTGTTGAGATGATACATACTATGTCTCTAATTCATGATGATTTGCCTTGTATGGATGACGACGAT    480
        ********************************************************************************

SlG2    CTCCGCCGTGGGAAGCCGACGAATCATAAAGTGTACGGTGAGGATGTGGCGGTCCTCGCCGGAGATGCGCTACTTGCTTT    560
slg2-1  CTCCGCCGTGGGAAGCCGACGAATCATAAAGTGTACGGTGAGGATGTGGCGGTCCTCGCCGGAGATGCGCTACTTGCTTT    560
slg2-2  CTCCGCCGTGGGAAGCCGACGAATCATAAAGTGTACGGTGAGGATGTGGCGGTCCTCGCCGGAGATGCGCTACTTGCTTT    560
        ********************************************************************************

SlG2    CGCATTCGAGTACCTCGCTACCGCTACAACCGGAGTTTCTCCGTCGAGGATCCTCGTTGCTGTCGCCGAATTGGCGAAAT    640
slg2-1  CGCATTCGAGTACCTCGCTACCGCTACAACCGGAGTTTCTCCGTCGAGGATCCTCGTTGCTGTCGCCGAATTGGCGAAAT    640
slg2-2  CGCATTCGAGTACCTCGCTACCGCTACAACCGGAGTTTCTCCGTCGAGGATCCTCGTTGCTGTCGCCGAATTGGCGAAAT    640
        ********************************************************************************

                          sgRNA-1                PAM
SlG2    CTGTTGGAACGGAAGGGTTAGTAGCTGGACAAGTAG--CGGATTTAGCTTGTACTGGTAACCCTAATGTGGGATTAGAAA    718
slg2-1  CTGTTGGAACGGAAGGGTTAGTAGCTGGACAAG-------------------------------------------------    673
slg2-2  CTGTTGGAACGGAAGGGTTAGTAGCTGGACAAGGCTAAGGAATTTAGCTTGTACTGGTAACCCTAATGTGGGATTAGAAA    720
        ********************************                    slg2-2

             EcoRI                                                sgRNA-2             PAM
SlG2    TGCTTGAATTCATTCACATACACAAAACGGCGGCGTTGCTAGAAGCTTCCGTTGTAATCGGAGCAATCCTCGGCGGCGGA    798
slg2-1  ---------------------------------------------------------------GGCGGCGGA    682
slg2-2  ---------------------------------------------------------------    720

SlG2    GCTGATGAAGAAGTGGATAAGTTAAGGAGATTTGCCCGATGCATCGGTTTATTGTTTCAGGTAGTTGATGATATCCTTGA    878
slg2-1  GCTGATGAAGAAGTGGATAAGTTAAGGAGATTTGCCCGATGCATCGGTTTATTGTTTCAGGTAGTTGATGATATCCTTGA    762
slg2-2  GCTGA-------------------------------------------------------------------------    720
        slg2-1

                                                          SIG2 CRISPR Geno R
SlG2    CGTGACAAAGTCGTCGTCGGAGCTCGGAAAAACCGCCGGAAAAGATTTGGCGGTTGATAAAACGACGTATCCGAAGCTGC    958
slg2-1  CGTGACAAAGTCGTCGTCGGAGCTCGGAAAAACCGCCGGAAAAGATTTGGCGGTTGATAAAACGACGTATCCGAAGCTGC    842
slg2-2  -----------------------------------------CGTTTGGCGGTTGATAAAACGACGTATCCGAAGCTGC    757
                                                   ***************************

SlG2    TGGGATTGGAAAAGGCTAAGGAATTTGCGGCGGAGCTCAACGGCGAAGCTAAACAACAGCTGGCGGCGTTTGATTCACAC    1038
slg2-1  TGGGATTGGAAAAGGCTAAGGAATTTGCGGCGGAGCTCAACGGCGAAGCTAAACAACAGCTGGCGGCGTTTGATTCACAC    922
slg2-2  TGGGATTGGAAAAGGCTAAGGAATTTGCGGCGGAGCTCAACGGCGAAGCTAAACAACAGCTGGCGGCGTTTGATTCACAC    837
        ********************************************************************************

SlG2    AAAGCTGCTCCATTGATTGCTTTAGCAGATTACATTGCTAATCGTCAAAATTAA    1092
slg2-1  AAAGCTGCTCCATTGATTGCTTTAGCAGATTACATTGCTAATCGTCAAAATTAA    976
slg2-2  AAAGCTGCTCCATTGATTGCTTTAGCAGATTACATTGCTAATCGTCAAAATTAA    891
        *****************************************************
```

Figure S6. DNA sequence alignment of *SIG2* CRISPR mutants. Alignment was performed using *Clustal Omega* (https://www.ebi.ac.uk/Tools/msa/clustalo/) with default settings. The sequence encoding the predicted plastid-targeting peptide is boxed in green. Designed single-guide RNAs (sgRNA) and genotyping oligonucleotides are highlighted in blue and purple, respectively. The designed sgRNAs encompass an *EcoRI* restriction site (underlined in black). Protospacer adjacent motifs (PAM) are highlighted in red. Translation stop codons are boxed and marked in bold. Sequences changes due to CRISPR-Cas9 are depicted in yellow. Numbers at the end of each sequence indicate DNA sequence length.

10

```
                                                            SIG3 CRISPR Geno F
SlG3    ATGAGTCTTTCAACAACAATTACAACTTGGGGATACACCCATCATCCCTTTTCTGACGTTGGAAATAAAGGCAGATCCAG 80
slg3-1  ATGAGTCTTTCAACAACAATTACAACTTGGGGATACACCCATCATCCCTTTTCTGACGTTGGAAATAAAGGCAGATCCAG 80
slg3-2  ATGAGTCTTTCAACAACAATTACAACTTGGGGATACACCCATCATCCCTTTTCTGACGTTGGAAATAAAGGCAGATCCAG 80
        ********************************************************************************

                                                                        sgRNA-1
SlG3    ATTTCGCTCTCCAGGATTCATGCCTCATCTGAAGATGAAATTCTTCACTAACCCTTCTTCTCTTTGTGTCTCAGCTCTTC 160
slg3-1  ATTTCGCTCTCCAGGATTCATGCCTCATCTGAAGATGAAATTCTTCACTAACCCTTCTTCTCTTTGTGTCTCAGCTCTTC 160
slg3-2  ATTTCGCTCTCCAGGATTCATGCCTCATCTGAAGATGAAATTCTTCACTAACCCTTCTTCTCTTTGTGTCTCAGCTCTTC 160
        ********************************************************************************

            PAM
SlG3    TTACAAAGGAGCAAGAAAGCAAGAGCAAGAAACAAGCAATGGAGTTTAAAGAATACGTTCTTGAAAAGGCTGTTTCTGTC 240
slg3-1  TTA----------------------------------------------------------------------------- 163
slg3-2  TTA----------------------------------------------------------------------------- 163
        ***
                            PstI                                    sgRNA-2
SlG3    AACAAGGCTTTGGAATCTGCAGTCTCTATCAAGGAACCGGTCATGATTCATGAGTCCATGAGGTACTCTCTTCTTGCTGG 320
slg3-1  -----------------------------------------------------------------------------TGG 166
slg3-2  ------------------------------------------------------------------------------GG 165
                                                                                     **
            PAM
SlG3    TGGGAAAAGAATTAGACCCATGTTGTGTATAGCTGCTTGTGAGCTTGTTGGTGGGGTTGAGTCCACAGCCATGCCAGCAG 400
slg3-1  TGGGAAAAGAATTAGACCCATGTTGTGTATAGCTGCTTGTGAGCTTGTTGGTGGGGTTGAGTCCACAGCCATGCCAGCAG 246
slg3-2  TGGGAAAAGAATTAGACCCATGTTGTGTATAGCTGCTTGTGAGCTTGTTGGTGGGGTTGAGTCCACAGCCATGCCAGCAG 245
        ***********        ***                *  ***************************************
                    slg3-2              slg3-1

SlG3    CTTGTGCTGTTGAAATGATTCACACCATGTCTTTGATTCATGATGACCTTCCTTGTATGGATAATGATGATCTTAGAAGA 480
slg3-1  CTTGTGCTGTTGAAATGATTCACACCATGTCTTTGATTCATGATGACCTTCCTTGTATGGATAATGATGATCTTAGAAGA 326
slg3-2  CTTGTGCTGTTGAAATGATTCACACCATGTCTTTGATTCATGATGACCTTCCTTGTATGGATAATGATGATCTTAGAAGA 325
        ********************************************************************************

                                                            SIG3 CRISPR Geno F
SlG3    GGGAAACCTACAAATCACAAGATTTATGGGGAGGATGTGGCTGTTTTAGCAGGGGATGCACTTCTTGCATTAGCCTTTGA 560
slg3-1  GGGAAACCTACAAATCACAAGATTTATGGGGAGGATGTGGCTGTTTTAGCAGGGGATGCACTTCTTGCATTAGCCTTTGA 406
slg3-2  GGGAAACCTACAAATCACAAGATTTATGGGGAGGATGTGGCTGTTTTAGCAGGGGATGCACTTCTTGCATTAGCCTTTGA 405
        ********************************************************************************

SlG3    GCACATTGCTACTCATACAAAAGGGGTTTCTTCTGATAGAATTGTGAGGGTGATTGGTGAGTTGGCGAAGTGTATTGGGG 640
slg3-1  GCACATTGCTACTCATACAAAAGGGGTTTCTTCTGATAGAATTGTGAGGGTGATTGGTGAGTTGGCGAAGTGTATTGGGG 486
slg3-2  GCACATTGCTACTCATACAAAAGGGGTTTCTTCTGATAGAATTGTGAGGGTGATTGGTGAGTTGGCGAAGTGTATTGGGG 485
        ********************************************************************************

SlG3    CAGAGGGACTTGTAGCTGGTCAGGTTGTAGATATAATTTCAGAAGGCATTTCTGATGTTGATTTGAAGCATTTAGAGTTC 720
slg3-1  CAGAGGGACTTGTAGCTGGTCAGGTTGTAGATATAATTTCAGAAGGCATTTCTGATGTTGATTTGAAGCATTTAGAGTTC 566
slg3-2  CAGAGGGACTTGTAGCTGGTCAGGTTGTAGATATAATTTCAGAAGGCATTTCTGATGTTGATTTGAAGCATTTAGAGTTC 565
        ********************************************************************************

SlG3    ATTCATCTGCACAAGACTGCAGCTTTGTTAGAAGGGTCAGTGGTGCTAGGGGCTATATTAGGAGGTGCACCAGATGAAGA 800
slg3-1  ATTCATCTGCACAAGACTGCAGCTTTGTTAGAAGGGTCAGTGGTGCTAGGGGCTATATTAGGAGGTGCACCAGATGAAGA 646
slg3-2  ATTCATCTGCACAAGACTGCAGCTTTGTTAGAAGGGTCAGTGGTGCTAGGGGCTATATTAGGAGGTGCACCAGATGAAGA 645
        ********************************************************************************

SlG3    TGTGGAAAAGCTAAGAAAATTTGCAAGATGTATTGGTTTGTTATTTCAAGTTGTGGATGATATTCTTGATGTCACAAAGT 880
slg3-1  TGTGGAAAAGCTAAGAAAATTTGCAAGATGTATTGGTTTGTTATTTCAAGTTGTGGATGATATTCTTGATGTCACAAAGT 726
slg3-2  TGTGGAAAAGCTAAGAAAATTTGCAAGATGTATTGGTTTGTTATTTCAAGTTGTGGATGATATTCTTGATGTCACAAAGT 725
        ********************************************************************************

SlG3    CTTCTCAGCAATTGGGGAAAACAGCTGGGAAGGACTTGGTTGCTGATAAGGTAACTTATCCCAAACTGATAGGTATTGAG 960
slg3-1  CTTCTCAGCAATTGGGGAAAACAGCTGGGAAGGACTTGGTTGCTGATAAGGTAACTTATCCCAAACTGATAGGTATTGAG 806
slg3-2  CTTCTCAGCAATTGGGGAAAACAGCTGGGAAGGACTTGGTTGCTGATAAGGTAACTTATCCCAAACTGATAGGTATTGAG 805
        ********************************************************************************

SlG3    AAATCTAGGGAGTTTGCTGAGGAGTTAAACAAAGAAGCGAAAGCTCAGCTTGTTGGATTTGATCAAGAGAAAGCAGCTCC 1040
slg3-1  AAATCTAGGGAGTTTGCTGAGGAGTTAAACAAAGAAGCGAAAGCTCAGCTTGTTGGATTTGATCAAGAGAAAGCAGCTCC 886
slg3-2  AAATCTAGGGAGTTTGCTGAGGAGTTAAACAAAGAAGCGAAAGCTCAGCTTGTTGGATTTGATCAAGAGAAAGCAGCTCC 885
        ********************************************************************************

SlG3    ATTGTTTGCTCTTGCAAATTATATTGCTTACAGAGAGAATTAA 1083
slg3-1  ATTGTTTGCTCTTGCAAATTATATTGCTTACAGAGAGAATTAA 929
slg3-2  ATTGTTTGCTCTTGCAAATTATATTGCTTACAGAGAGAATTAA 928
        *******************************************
```
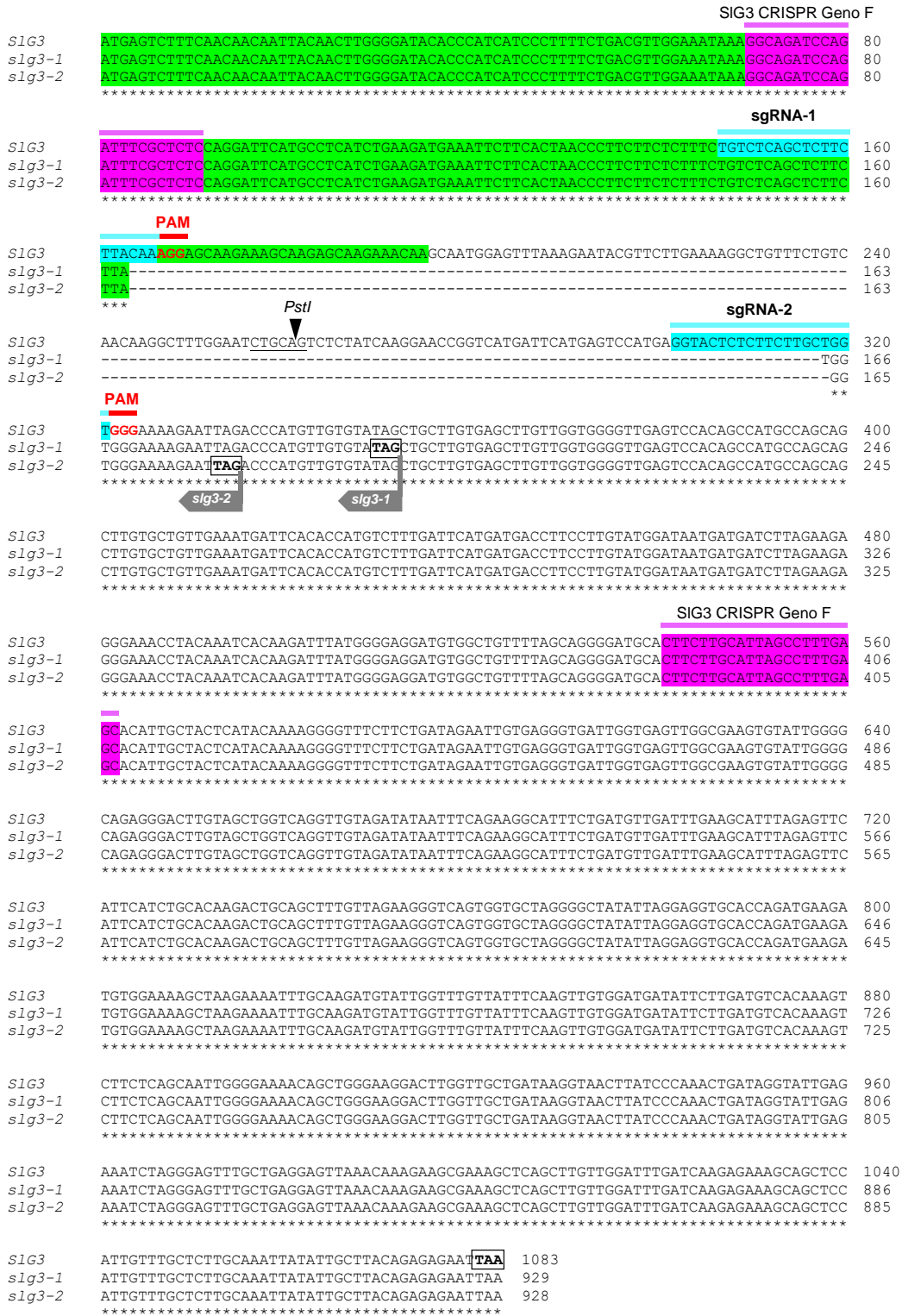
Figure S7. DNA sequence alignment of *SIG3* CRISPR mutants. Alignment was performed using *Clustal Omega* (https://www.ebi.ac.uk/Tools/msa/clustalo/) with default settings. The sequence encoding the predicted plastid-targeting peptide is boxed in green. Designed single-guide RNAs (sgRNA) and genotyping oligonucleotides are highlighted in blue and purple, respectively. The designed sgRNAs encompass a *PstI* restriction site (underlined in black). Protospacer adjacent motifs (PAM) are highlighted in red. Translation stop codons are boxed and marked in bold. Numbers at the end of each sequence indicate DNA sequence length.

A

B

Figure S8. Protein alignments of WT and mutant SIG2 (A) and SIG3 (B) sequences. *Clustal Omega* (https://www.ebi.ac.uk/Tools/msa/clustalo/) with default settings was used for the alignment. The predicted targeting peptide, the region of the designed sgRNAs and the catalytic motifs FARM and SARM are boxed in green, blue and black, respectively. The protein-protein interaction CxxxC motifs (x = any hydrophobic residue) are highlighted in pink. Numbers at the end of each sequence indicate protein length.
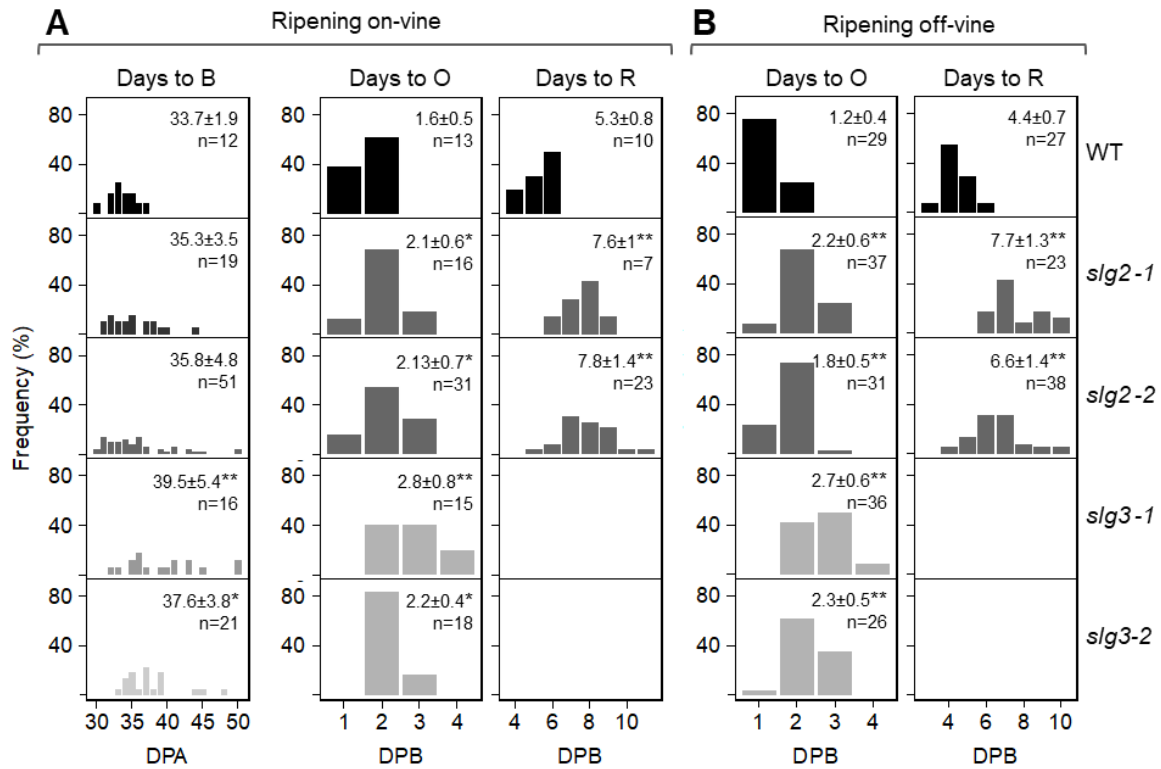
Figure S9. Fruit ripening initiation and progression in WT and mutant plants.
Histograms represent the number of days to reach Breaker (B), Orange (O) and Red (R) fruit stages represented as days post-anthesis (DPA) or days post-breaker (DPB). On-vine **(A)** and off-vine **(B)** measurements are shown. For on-vine measurements, flowers were marked in anthesis and followed *in planta*. For off-vine measurements fruits were harvested at the B stage. The mean±SD values and the sample size (n) are shown in each histogram. Asterisks indicate statistically significant differences among means relative to WT samples (one-way ANOVA followed by Dunnett's multiple comparisons test, *$p < 0.05$, **$p < 0.01$).
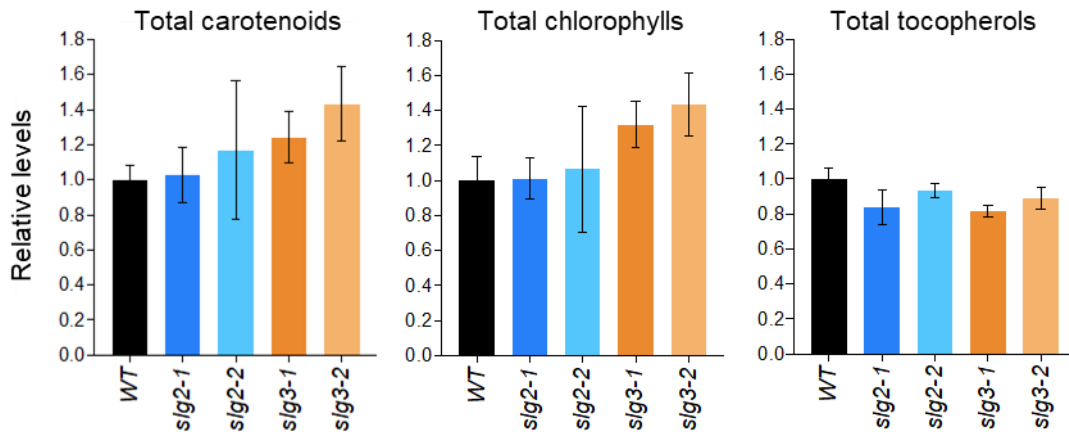
Figure S10. Relative levels of plastidial isoprenoids in mature green fruits from WT and mutant lines. Values correspond to the mean±SD of at least three independent biological replicates (n=3) relative to WT levels. No statistically significant differences among means were found (one-way ANOVA).
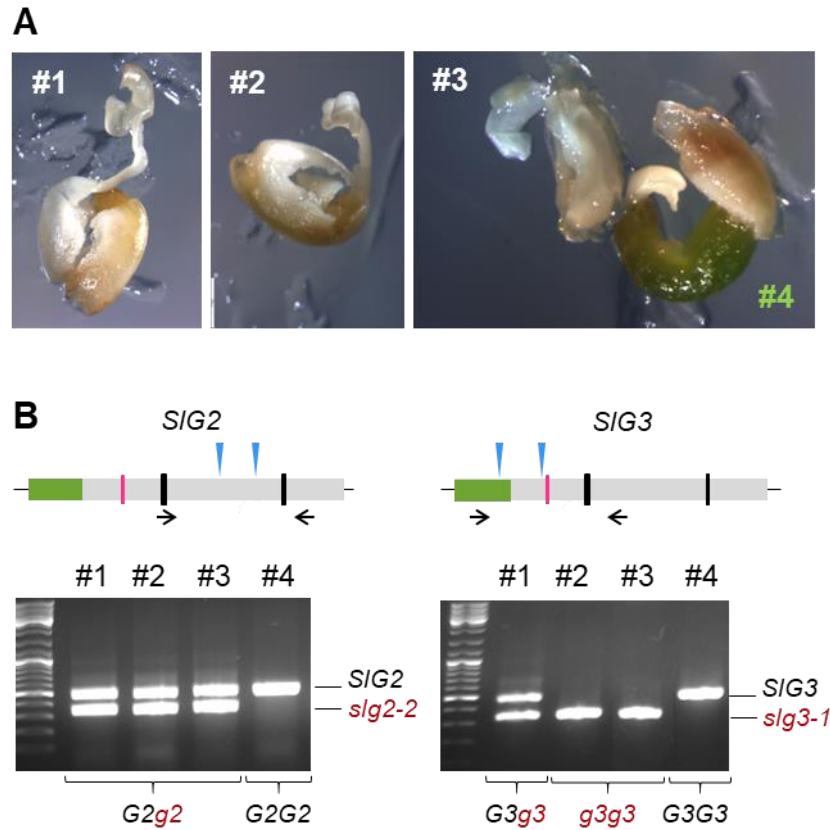
Figure S11. PCR-based genotyping of non-germinating F2 seeds from the cross of *slg2-2* and *slg3-1* mutant plants. (A) Non-germinating seeds were manually open to show the phenotype of their embryos. Only seed #4 showed a green embryo. **(B)** Scheme representing the *SlG2* and *SlG3* genes and the genotyping results. Blue arrowheads indicate the position of the designed sgRNAs to generate deletions, and black arrows represent primer pairs used for PCR-based genotyping. Gel pictures show the PCR amplification products from samples of the embryos shown in (A). The position of amplicons from WT and mutant genes (in black and red, respectively) is indicated.

TABLES S1-S11– see Excel file